



OPEN

Anodic electrosynthesis of MIL-53(Al)-N(CH₂PO₃H₂)₂ as a mesoporous catalyst for synthesis of novel (*N*-methyl-pyrrol)-pyrazolo[3,4-*b*]pyridines via a cooperative vinylogous anomeric based oxidation

Sima Kalhor¹, Mahmoud Zarei¹, Mohammad Ali Zolfigol¹, Hassan Sepehrmansourie¹, Davood Nematollahi², Saber Alizadeh², Hu Shi³ & Jalal Arjomandi⁴

In this paper, the MIL-53(Al)-NH₂ metal–organic frameworks (MOFs) was prepared based on the anodic electrosynthesis under green conditions. The anodic electrosynthesis as an environmentally friendly procedure was performed in the aqueous solution, room temperature, atmospheric pressure, and in the short reaction time (30 min). Also, the employed procedure was accomplished without the need for the ex-situ salt and base/probase additives as cation source and ligand activating agent at the constant current mode (10.0 mA cm⁻²). The electrosynthesized MOFs was functionalized with phosphorus acid tags as a novel mesoporous catalyst. This mesoporous catalyst was successfully employed for synthesis of new series (*N*-methyl-pyrrol)-pyrazolo[3,4-*b*]pyridines by one-pot condensation reaction of 3-methyl-1-phenyl-1*H*-pyrazol-5-amine, 3-(1-methyl-1*H*-pyrrol-2-yl)-3-oxopropanenitrile and various aromatic aldehydes (mono, bis and tripodal). This catalyst proceeded the organic synthetic reaction via a cooperative vinylogous anomeric based oxidation mechanism with a marginal decreasing its catalytic activity after recycling and reusability.

Metal–organic frameworks (MOFs) have been employed in various fields such as catalysts, electrocatalysts, supercapacitors, drug delivery, sensors, batteries, membranes, and absorbents due to the eye-catching features such as various synthesis methods, structural diversity, high surface area, and attractive architectures^{1–14}. Besides, the potential functionalization and post-modification of MOFs have exposed the art of chemists in different fields^{15,16}. The various documents have been reported for synthesis and electrosynthesis of MOFs as powder and thin films^{17–29}. Behind the beneficial chemical synthesis procedures, the anodic and cathodic electrosynthesis methods are easy to observe and have been received a more acceptable niche and platform because of the environmentally friendly conditions^{30–34}. This prominent glance comes from the one-step, green, and mild strategy that use of renewable electricity source instead of high temperature and high vacuum/pressure as a driving agent^{30–34}. One of the MOFs having been synthesized via chemical and electrochemical procedures is MIL-53-(Al)-NH₂,

¹Department of Organic Chemistry, Faculty of Chemistry, Bu-Ali Sina University, PO Box 6517838683, Hamedan, Iran. ²Department of Analytical Chemistry, Faculty of Chemistry, Bu-Ali Sina University, PO Box 6517838683, Hamedan, Iran. ³School of Chemistry and Chemical Engineering, Institute of Molecular Science, Shanxi University, Taiyuan 030006, China. ⁴Department of Physical Chemistry, Faculty of Chemistry, Bu-Ali Sina University, PO Box 6517838683, Hamedan, Iran. ✉email: mahmoud8103@yahoo.com; zolfi@basu.ac.ir; nemat@basu.ac.ir; s.alizadeh93@basu.ac.ir; hshi@sxu.edu.cn

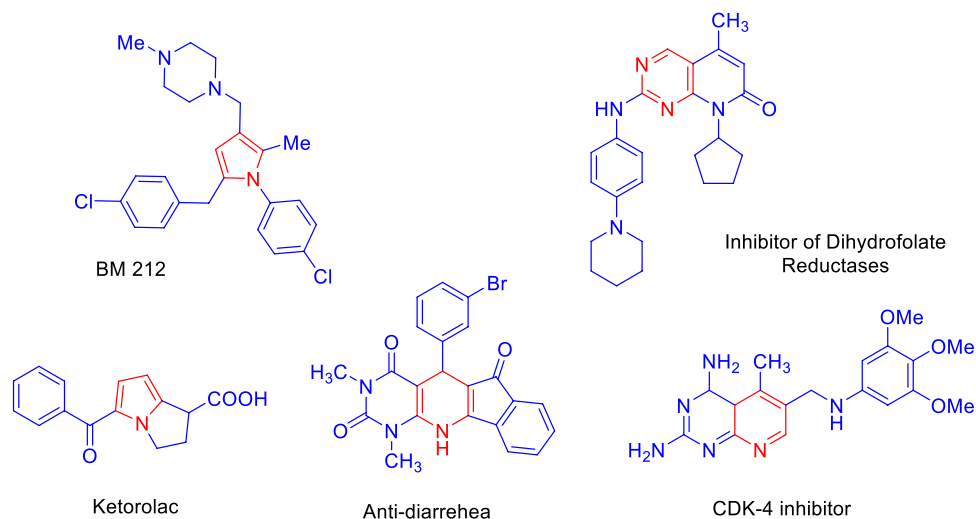


Figure 1. Structure of *N*-heterocycle rings as drug candidates.

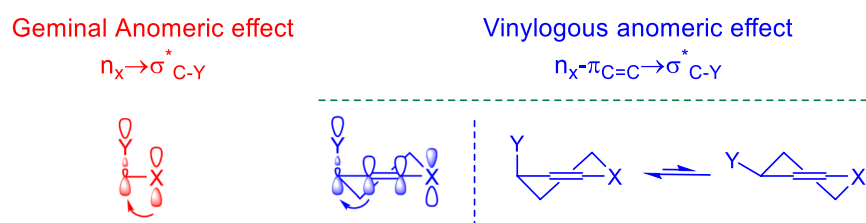


Figure 2. Geminal anomeric effect versus vinylogous anomeric effect⁶¹.

which has been used in different applications^{35–41}. The main drawbacks of conventional chemical methods are the critical synthesis conditions such as high-pressure or -vacuum, prolonged time, and high temperature^{38–41}. While, the anodic electro-synthesis method provides a mild and greener condition for this purpose^{35–37}. In this method the anodic electrode plays the role of cation source for avoiding using of related cation salt which leads to the prevention of pore-blocking by the salt ions. Also, the electroreduction of water molecules on the counter electrode generates the hydroxide ions that lead to the in-situ deprotonation of ligands without the need for any ex-situ base/probase additive. Finally, the coordination and crystallization of MOF can be progressed by a green electricity source instead of high vacuum/pressure as a driving agent^{30–34}. At the next step, the electro-synthesized MOFs was functionalized by phosphorous acid tags. Organophosphoric acid as a catalyst has been used for the oligomerization of light olefins, destructive alkylation of hydrocarbons and organic synthesis^{42,43}. Furthermore, phosphoric acid and its derivatives have been also used in multinuclear NMR, adsorption and extraction⁴⁴. Materials containing $N(CH_2PO_3H_2)_2$ moieties have environmental impacts worldwide in agricultural, chemical, and pharmaceutical applications^{45,46}. Recently efficient methodologies have been reported for the preparation of metal-organic frameworks^{47,48}, melamine and glycoluril^{49,50} and mesoporous materials (SBA-15) with phosphorous acid functional groups⁵¹.

Lots of researches have been done to achieve a novel pyridine and other derivatives as drug candidates^{52,53}. Aryl and heterocyclic compounds substituted with β -ketonitriles have shown a unique class of useful intermediates. Pyran, pyridine and other ring derivatives plays important role in nature and drug development. Molecules with pyran and pyridine moieties are also associated with several important biological and pharmacological activities such as antitumor, antipyretic, analgesic, antiallergic, anti-hypertension, bronchitis dilator, strengthen the heart, blood vessel dilator, antimalarial, anti-fungal, an adenosine kinase inhibitor, diuretic, tyrosine kinas' inhibitors and antibacterial activity^{54–59}. Furthermore, these materials were also applied in the synthesis of BM 212, Ketorolac and other compounds as anti-fungal and anti-bacterial, and anti-inflammatory inhibitors of dihydrofolate reductases, anti-diarrhoea and CDK-4 inhibitor respectively (Fig. 1)⁶⁰.

The anomeric interactions extended through double bonds has been named as a vinylogous anomeric effect. The geminal anomeric effect is compared with vinylogous anomeric (Fig. 2). As it can be seen in Fig. 2, in the vinylogous anomeric effect electron density is shared through a double bond but in the geminal anomeric effect donor and acceptor are germinal⁶¹. Recently anomeric based oxidation has been introduced for the latter step at the synthesis of susceptible molecules^{62,63}. Since that reduction of substrates by NADH and NADPH₂ have proceeded via a hydride transfer^{64–66}. The key feature of the reduction mechanism is hydride transfer from carbon via an anomeric based oxidation mechanism. Herein, two cooperative vinylogous anomeric based oxidation

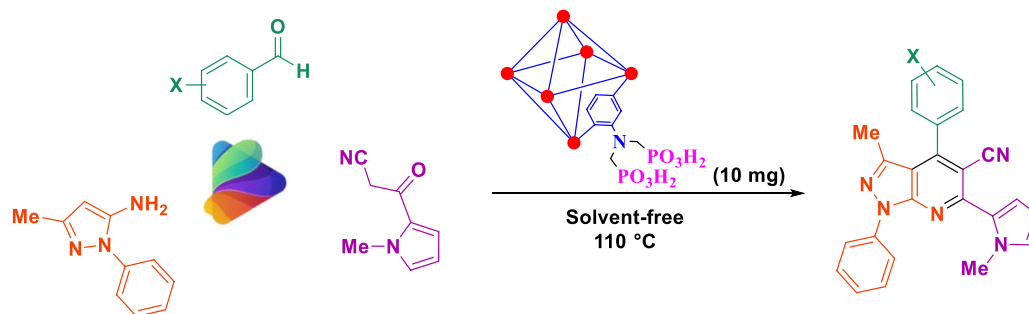


Figure 3. Synthesis of new (*N*-methyl-pyrrol)-pyrazolo[3,4-*b*]pyridines using MIL-53(Al)-N(CH₂PO₃H₂)₂.

mechanisms were suggested for the synthesis of new molecules with pyridine structure in the presence and absence of oxygen^{67,68}.

Since molecules with indole moieties are biological interest candidates⁶⁹ and our background on the comprehensive reviewing of bis and tris indolyl methanes⁷⁰, we decided to synthesis pyridines with both indole and pyrazole moieties. Therefore, in continuation of our investigations on the development of electro-synthesis of metal–organic frameworks (MOFs) and its chemical post-functionalization with phosphorous acid tags^{47–51}, herein we wish to report a green methodology for preparing of new MIL-53(Al)-N(CH₂PO₃H₂)₂ as an efficient mesoporous catalyst. For this purpose, the MIL-53-(Al)-NH₂ was successfully fabricated via anodic electro-synthesis technique in the aqueous solution, short reaction time (30 min), room temperature, and atmospheric pressure at the constant current mode (10.0 mA cm⁻²). It should be noted that the employed procedure was accomplished without the need for the related cation salt as a cation source and ex-situ base/probase additive for deprotonation of the ligand. The final mesoporous catalyst was prepared through functionalizing of MIL-53-(Al)-NH₂ with the phosphorous acid tags and utilized for the synthesis of new (*N*-methyl-pyrrol)-pyrazolo[3,4-*b*]pyridines by the condensation reaction of 3-methyl-1-phenyl-1*H*-pyrazol-5-amine, 3-(1-methyl-1*H*-pyrrol-2-yl)-3-oxopropanenitrile and various aromatic aldehydes (mono, bis and tripodal) under green conditions (Fig. 3).

Experimental

Materials. 2-Amino terephthalic acid (NH₂-H₂BDC) (Merck, 95%), potassium nitrate (KNO₃) (Sigma-Aldrich, 99%), DMF (Merck, 99%), phosphorous acid (Merck, 99%), 1-methyl-1*H*-pyrrole (Merck, 98%), 2-cyanoacetic acid (Merck, 98%), EtOH (Merck, 99%) were reagent-grade materials and employed as received without further purification.

Instrumental measurements. From the model of the BRUKER Ultrashield FT-NMR spectrometer (δ in ppm) were recorded ¹H NMR (600 or 400 MHz), ¹³C NMR (151 or 101 MHz). Recorded on a Büchi B-545 apparatus in open capillary tubes were melting points. The PerkinElmer PE-1600-FTIR device was recorded for infrared spectra of compounds. SEM was performed using a scanning electron microscope for field publishing made by TE-SCAN. Thermal gravimetry (TG) and differential thermal gravimetric (DTG) were analyzed by a Perkin Elmer (Model: Pyris 1). BET and BJH were analyzed by BELSORP-mini ii high precision Surface area and pore size. Xrd was analyzed by ITAL STRUCTURE APD2000.

General procedure for the anodic electro-synthesis of MIL-53(Al)-NH₂. In a typical anodic electro-synthesis procedure, (0.1 mmol, 0.127 g) potassium nitrate (KNO₃) as a supporting electrolyte was dissolved in 45.0 mL distilled water (Solution A). Also, (8.2 mmol, 1.5 g) of 2-amino terephthalic acid (NH₂-H₂BDC) as a ligand was dissolved in the 5.0 mL EtOH (solution B) and added to solution A (10 Vol% EtOH). The precursor was stirred at room temperature for 15 min before the electro-synthesis. In the following, the prepared precursor transferred to the homemade undivided two-electrode cell consists of a cap glass bottle and two Aluminum plates (100.0 mm × 30.0 mm × 2.0 mm) as working (cation source) and the auxiliary electrodes. Electro-synthesis of MOF was performed by applying 10.0 mA cm⁻² current densities for 30 min. The MIL-53-(Al)-NH₃ powders were removed from the solution by centrifuge at 5000 rpm for 5 min and rinsed twice with distilled water and DMF. The final MIL-53-(Al)-NH₃ was aged overnight at 100 °C.

General procedure for the preparation of MIL-53(Al)-N(CH₂PO₃H₂)₂. In a 50 mL round-bottomed flask, MIL-53(Al)-NH₂ (0.5 g), paraformaldehyde (5.0 mmol, 0.27 g), phosphorous acid (4.0 mmol, 0.76 g), *p*-TSA (0.5 mmol, 0.08 g) and ethanol (25 mL) were added and refluxed for 18 h. After this time, a yellow precipitated was filtered off by centrifugation (1000 rpm, 10 min). The obtained solid residue was dried under vacuum to give MIL-53(Al)-N(CH₂PO₃H₂)₂ (Fig. 4).

General procedure for the synthesis of 3-methyl-6-(1-methyl-1*H*-pyrrol-3-yl)-1,4-diphenyl-1*H*-pyrazolo[3,4-*b*]pyridine-5-carbonitrile derivatives using MIL-53(Al)-N(CH₂PO₃H₂)₂ as the catalyst. At first 3-(1-methyl-1*H*-pyrrol-2-yl)-3-oxopropanenitrile was synthesized according to the previously reported literature (Fig. 5)⁷¹. Then, a mixture of 3-methyl-1-phenyl-1*H*-pyrazol-5-amine (1.0 mmol,

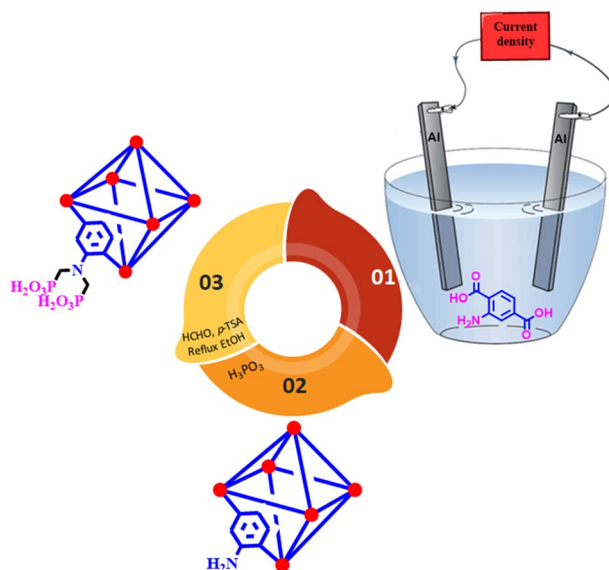


Figure 4. Preparation of MIL-53(Al)-N(CH₂PO₃H₂)₂.

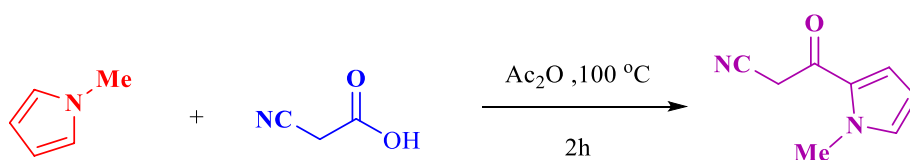


Figure 5. Preparation of 3-(1-methyl-1H-pyrrol-2-yl)-3-oxopropanenitrile.

0.174 g), aryl aldehyde (1.0 mmol), 3-(1-methyl-1H-pyrrol-2-yl)-3-oxopropanenitrile (1.0 mmol, 0.148 g) and MIL-53(Al)-N(CH₂PO₃H₂)₂ (10.0 mg) as catalyst were stirred under solvent-free conditions at 110 °C in a 25.0 mL round-bottomed. After completion of the reaction (monitor by TLC *n*-hexane: ethyl acetate; 7:3). The catalyst was separated by centrifugation (2000 rpm) after adding PEG (5.0 mL) for 5 min. Finally, the mixture was filtered off and washed with ethanol (3 × 10 mL) and the final pure product was obtained (Fig. 3).

Spectral data. 3-methyl-6-(1-methyl-1H-pyrrol-2-yl)-1-phenyl-4-(*p*-tolyl)-1H-pyrazolo[3,4-*b*]pyridine-5-carbonitrile (1a). White solid; M.p: 216–218 °C; FT-IR (KBr): ν (cm⁻¹) = 3282, 2955, 2923, 2219, 1575, 1556, 1506, 1488, 1415. ¹H NMR (600 MHz, DMSO-*d*₆) δ 8.13 (d, *J* = 7.8 Hz, 2H), 7.60 (t, *J* = 7.9 Hz, 2H), 7.54 (d, *J* = 7.9 Hz, 2H), 7.45 (d, *J* = 7.8 Hz, 2H), 7.40 (t, *J* = 7.4 Hz, 1H), 7.13 (s, 1H), 6.99 (dd, *J* = 3.8, 1.4 Hz, 1H), 6.21 (dd, *J* = 3.6, 2.7 Hz, 1H), 3.94 (s, 3H), 2.46 (s, 3H), 2.05 (s, 3H). ¹³C NMR (151 MHz, DMSO-*d*₆) δ 153.4, 152.4, 149.7, 144.40, 140.0, 138.5, 131.3, 129.7, 129.5, 129.3, 129.0, 128.6, 127.0, 121.8, 118.4, 115.9, 112.5, 108.1, 101.0, 39.5, 36.9, 21.4, 14.9, (See SI, Figs. S1–S3).

4-(4-isopropylphenyl)-3-methyl-6-(1-methyl-1H-pyrrol-2-yl)-1-phenyl-1H-pyrazolo[3,4-*b*]pyridine-5-carbonitrile (2a). White solid; M.p: 193–195 °C; FT-IR (KBr): ν (cm⁻¹) = 3067, 2959, 2929, 2866, 2221, 1572, 1558, 1541, 1507, 1415. ¹H NMR (600 MHz, DMSO-*d*₆) δ 8.13 (d, *J* = 7.7 Hz, 2H), 7.60 (t, *J* = 7.9 Hz, 2H), 7.57 (d, *J* = 8.1 Hz, 2H), 7.51 (d, *J* = 8.1 Hz, 2H), 7.40 (t, *J* = 7.4 Hz, 1H), 7.13 (s, 1H), 6.99 (dd, *J* = 3.8, 1.5 Hz, 1H), 6.21 (dd, *J* = 3.7, 2.7 Hz, 1H), 3.94 (s, 3H), 3.05 (d, *J* = 6.9 Hz, 1H), 2.04 (s, 3H), 1.31 (d, *J* = 6.9 Hz, 6H). ¹³C NMR (151 MHz, DMSO-*d*₆) δ 153.3, 152.5, 150.7, 149.7, 144.4, 138.5, 131.5, 129.7, 129.5, 129.0, 128.6, 127.0, 126.8, 121.8, 118.4, 115.9, 112.6, 108.1, 100.9, 36.9, 33.7, 24.2, 14.8, (See SI, Figs. S4–S6).

4-(4-methoxyphenyl)-3-methyl-6-(1-methyl-1H-pyrrol-2-yl)-1-phenyl-1H-pyrazolo[3,4-*b*]pyridine-5-carbonitrile (3a). White solid; M.p: 208–210 °C; FT-IR (KBr): ν (cm⁻¹) = 3018, 2974, 2933, 2838, 2119, 1609, 1577, 1558, 1513, 1437, 1415. ¹H NMR (600 MHz, DMSO-*d*₆) δ 8.12 (d, *J* = 7.9 Hz, 2H), 7.59 (d, *J* = 8.1 Hz, 3H), 7.39 (t, *J* = 7.4 Hz, 1H), 7.18 (d, *J* = 8.6 Hz, 2H), 7.12 (s, 1H), 6.99 (dd, *J* = 3.7, 1.3 Hz, 1H), 6.22–6.20 (m, 1H), 3.94 (s, 3H), 3.89 (s, 3H), 2.08 (s, 3H). ¹³C NMR (151 MHz, DMSO-*d*₆) δ 160.9, 153.2, 152.5, 149.7, 144.4, 138.6, 131.1, 129.7, 128.9, 128.6, 127.0, 126.1, 121.7, 118.5, 115.9, 114.3, 112.7, 108.1, 101.1, 55.7, 36.9, 15.0, (See SI, Figs. S7–S9).

4-(3,4-dimethoxyphenyl)-3-methyl-6-(1-methyl-1H-pyrrol-2-yl)-1-phenyl-1H-pyrazolo[3,4-*b*]pyridine-5-carbonitrile (4a). White solid; M.p: 196–198 °C; FT-IR (KBr): ν (cm⁻¹) = 3128, 2992, 2960, 2834, 2224, 1600, 1568,

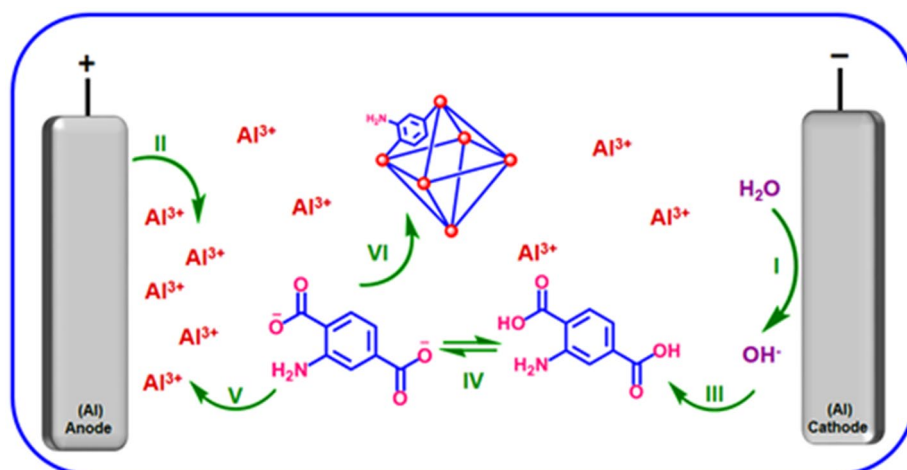


Figure 6. Preparation of MIL-53(Al)-NH₂ using anodic electro-synthesis method.

1516, 1490, 1439. ¹H NMR (400 MHz, DMSO-*d*₆) δ 8.13 (d, *J*=7.7 Hz, 2H), 7.61 (t, *J*=7.9 Hz, 2H), 7.40 (t, *J*=7.4 Hz, 1H), 7.28 (s, 1H), 7.20 (s, 2H), 7.13 (s, 1H), 7.00 (dd, *J*=3.8, 1.4 Hz, 1H), 6.22 (dd, *J*=3.7, 2.7 Hz, 1H), 3.94 (s, 3H), 3.89 (s, 3H), 3.83 (s, 3H), 2.13 (s, 3H). ¹³C NMR (101 MHz, DMSO-*d*₆) δ 152.7, 152.0, 149.8, 149.2, 148.2, 144.0, 138.1, 129.2, 128.4, 128.1, 126.5, 125.7, 121.8, 121.3, 118.0, 115.4, 112.7, 112.2, 111.2, 107.6, 100.7, 55.7, 55.5, 36.4, 14.5, (See SI, Figs. S10–S12).

3-methyl-6-(1-methyl-1H-pyrrol-2-yl)-1,4-diphenyl-1H-pyrazolo[3,4-b]pyridine-5 carbonitrile (5a). Brown solid; M.p: 174–178 °C; FT-IR (KBr): ν (cm⁻¹)=2961, 2923, 2216, 1656, 1599, 1567, 1506, 1487, 1415. ¹H NMR (400 MHz, DMSO-*d*₆) δ 8.15–8.10 (m, 2H), 7.65–7.64 (m, 4H), 7.61–7.58 (m, 2H), 7.44–7.36 (m, 1H), 7.14 (dd, *J*=2.6, 1.7 Hz, 1H), 7.00 (dd, *J*=3.9, 1.7 Hz, 1H), 6.22 (dd, *J*=3.9, 2.6 Hz, 1H), 3.95 (s, 3H), 2.02 (s, 3H). ¹³C NMR (101 MHz, DMSO-*d*₆) δ 152.7, 151.9, 149.2, 143.8, 138.0, 133.7, 129.8, 129.2, 128.8, 128.5, 128.4, 128.1, 126.6, 121.3, 117.8, 115.5, 112.0, 107.6, 100.4, 36.4, 14.2, (See SI, Figs. S13–S15).

4-(4-bromophenyl)-3-methyl-6-(1-methyl-1H-pyrrol-2-yl)-1-phenyl-1H-pyrazolo[3,4-b]pyridine-5-carbonitrile (6a). White solid; M.p: 235–237 °C; FT-IR (KBr): ν (cm⁻¹)=3063, 2983, 2953, 2214, 1995, 1574, 1557, 1506, 1485, 1412. ¹H NMR (600 MHz, DMSO-*d*₆) δ 8.12 (d, *J*=7.9 Hz, 2H), 7.86 (d, *J*=8.3 Hz, 2H), 7.64–7.59 (m, 4H), 7.40 (t, *J*=7.4 Hz, 1H), 7.14 (s, 1H), 7.00 (dd, *J*=3.8, 1.4 Hz, 1H), 6.22–6.21 (m, 1H), 3.94 (s, 3H), 2.06 (s, 3H). ¹³C NMR (151 MHz, DMSO-*d*₆) δ 152.4, 151.9, 149.7, 144.2, 138.5, 135.3, 133.0, 131.4, 129.7, 129.1, 129.1, 128.5, 127.1, 121.8, 118.2, 116.0, 112.4, 108.2, 100.9, 39.5, 36.9, 14.8, (See SI, Figs. S16–S18).

4-(4-chlorophenyl)-3-methyl-6-(1-methyl-1H-pyrrol-2-yl)-1-phenyl-1H-pyrazolo[3,4-b]pyridine-5-carbonitrile (7a). White solid; M.p: 238–240 °C; FT-IR (KBr): ν (cm⁻¹)=3083, 2980, 2964, 2216, 1595, 1573, 1555, 1506, 1486, 1413. ¹H NMR (600 MHz, DMSO-*d*₆) δ 8.12 (d, *J*=7.8 Hz, 2H), 7.71 (q, *J*=8.6 Hz, 4H), 7.61 (t, *J*=7.9 Hz, 2H), 7.40 (t, *J*=7.4 Hz, 1H), 7.14 (s, 1H), 7.00 (dd, *J*=3.8, 1.5 Hz, 1H), 6.22 (dd, *J*=3.7, 2.7 Hz, 1H), 3.94 (s, 3H), 2.06 (s, 3H). ¹³C NMR (151 MHz, DMSO-*d*₆) δ 152.4, 151.9, 149.7, 144.2, 138.5, 135.3, 133.0, 131.4, 129.7, 129.1, 129.1, 128.5, 127.1, 121.8, 118.2, 116.0, 112.43, 108.2, 100.9, 36.9, 14.8, (See SI, Figs. S19–S21).

4-(4-Fluorophenyl)-3-methyl-6-(1-methyl-1H-pyrrol-2-yl)-1-phenyl-1H-pyrazolo[3,4-b]pyridine-5-carbonitrile (8a). Light yellow solid; M.p: 241–243 °C; FT-IR (KBr): ν (cm⁻¹)=3070, 2960, 2226, 1602, 1563, 1506, 1486, 1412. ¹H NMR (400 MHz, DMSO-*d*₆) δ 8.13 (d, *J*=7.8 Hz, 2H), 7.60 (t, *J*=7.9 Hz, 2H), 7.54 (d, *J*=7.9 Hz, 2H), 7.45 (d, *J*=7.8 Hz, 2H), 7.40 (t, *J*=7.4 Hz, 1H), 7.13 (s, 1H), 6.99 (dd, *J*=3.8, 1.4 Hz, 1H), 6.21 (dd, *J*=3.6, 2.7 Hz, 1H), 3.94 (s, 3H), 2.46 (s, 3H), 2.05 (s, 3H). ¹³C NMR (101 MHz, DMSO-*d*₆) δ 164.1, 161.7, 151.9, 151.75, 149.2, 143.8, 138.0, 131.4, 131.4, 130.0, 129.3, 128.6, 128.0, 126.6, 121.3, 117.83, 115.7, 115.5, 115.4, 112.1, 107.7, 100.6, 36.4, 14.3, (See SI, Figs. S22–S24).

3-Methyl-6-(1-methyl-1H-pyrrol-2-yl)-1-phenyl-4-(pyridin-4-yl)-1H-pyrazolo[3,4-b]pyridine-5-carbonitrile (9a). Pale orange solid; M.p: 218–220 °C; FT-IR (KBr): ν (cm⁻¹)=3041, 2958, 2233, 1596, 1568, 1554, 1540, 1505, 1413. ¹H NMR (400 MHz, DMSO-*d*₆) δ 8.87 (dd, *J*=4.4, 1.6 Hz, 2H), 8.14–8.09 (m, 2H), 7.72 (dd, *J*=4.4, 1.6 Hz, 2H), 7.61 (t, *J*=8.0 Hz, 2H), 7.41 (t, *J*=7.4 Hz, 1H), 7.17–7.14 (m, 1H), 7.02 (dd, *J*=3.9, 1.7 Hz, 1H), 6.23 (dd, *J*=3.9, 2.6 Hz, 1H), 3.95 (s, 3H), 2.04 (s, 3H). ¹³C NMR (101 MHz, DMSO-*d*₆) δ 151.8, 149.8, 149.6, 149.1, 143.5, 141.7, 137.9, 129.3, 129.2, 128.8, 127.9, 126.7, 123.5, 121.3, 119.9, 117.4, 115.6, 111.2, 107.8, 99.81, 36.5, 14.1, (See SI, Figs. S25–S27).

4-(4-(Dimethylamino)phenyl)-3-methyl-6-(1-methyl-1H-pyrrol-2-yl)-1-phenyl-1H-pyrazolo[3,4-b]pyridine-5-carbonitrile (10a). Yellow solid; M.p: 248–250 °C; FT-IR (KBr): ν (cm⁻¹)=3107, 2906, 2814, 2220,

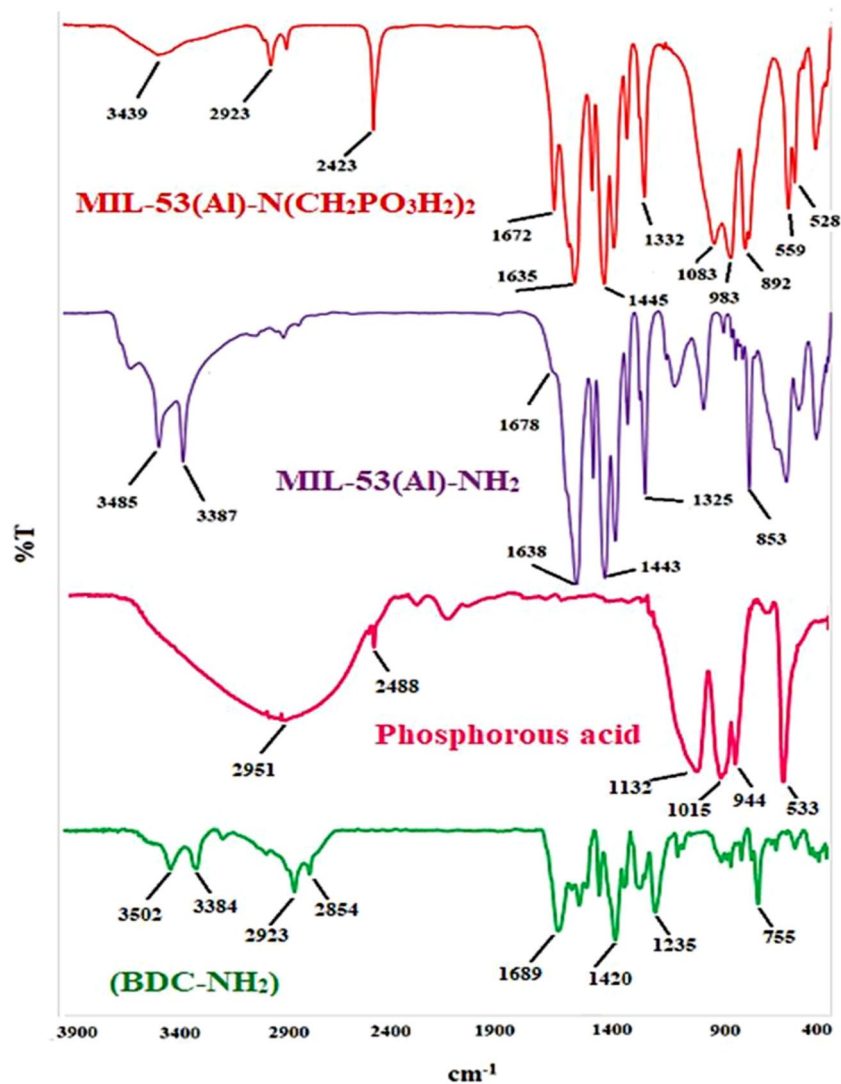


Figure 7. FT-IR analysis of 2-amino terephthalic acid, phosphorous acid, MIL-53(Al)-NH₂ and MIL-53(Al)-N(CH₂PO₃H₂)₂.

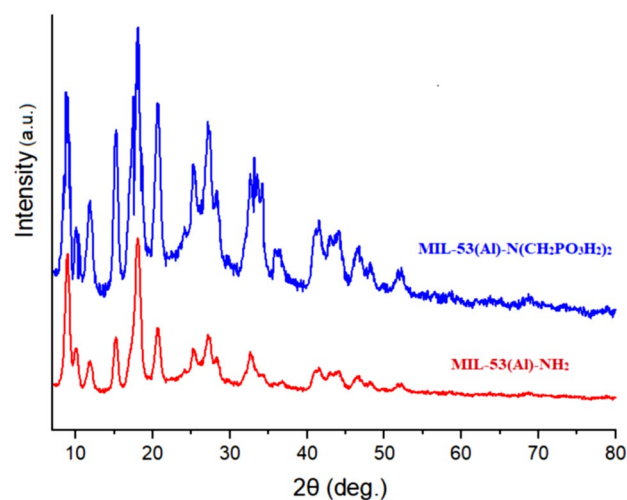


Figure 8. XRD pattern of MIL-53(Al)-NH₂ and MIL-53(Al)-N(CH₂PO₃H₂)₂.

1605, 1530, 1504, 1486. ¹H NMR (400 MHz, DMSO-*d*₆) δ 8.16–8.07 (m, 2H), 7.59 (t, *J* = 8.0 Hz, 2H), 7.51–7.44 (m, 2H), 7.43–7.34 (m, 1H), 7.10 (t, *J* = 2.1 Hz, 1H), 6.97 (dd, *J* = 3.9, 1.7 Hz, 1H), 6.93–6.86 (m, 2H), 6.20 (dd, *J* = 3.9, 2.6 Hz, 1H), 3.92 (s, 3H), 3.04 (s, 6H), 2.16 (s, 3H), (See SI, Figs. S28–S29).

4-(4-(Diethylamino)phenyl)-3-methyl-6-(1-methyl-1H-pyrrol-2-yl)-1-phenyl-1H-pyrazolo[3,4-b]pyridine-5-carbonitrile (11a). Orange solid; M.p: 186–188 °C; FT-IR (KBr): ν (cm⁻¹) = 2969, 2894, 2870, 2213, 1604, 1568, 1521, 1506, 1484. ¹H NMR (400 MHz, DMSO-*d*₆) δ 8.12 (d, *J* = 7.7 Hz, 2H), 7.59 (t, *J* = 7.9 Hz, 2H), 7.45 (d, *J* = 8.8 Hz, 2H), 7.38 (t, *J* = 7.4 Hz, 1H), 7.11–7.09 (m, 1H), 6.97 (dd, *J* = 3.9, 1.6 Hz, 1H), 6.84 (d, *J* = 8.9 Hz, 2H), 6.20 (dd, *J* = 3.8, 2.6 Hz, 1H), 3.92 (s, 3H), 3.45 (q, *J* = 6.9 Hz, 4H), 2.19 (s, 3H), 1.17 (t, *J* = 7.0 Hz, 6H). ¹³C NMR (101 MHz, DMSO-*d*₆) δ 153.5, 152.3, 149.4, 148.5, 144.0, 138.1, 130.9, 129.2, 128.3, 128.1, 126.4, 121.2, 118.9, 118.6, 115.3, 112.1, 110.3, 107.5, 100.1, 43.6, 36.3, 15.0, 12.3, (See SI, Figs. S30–S32).

4-(1H-Indol-3-yl)-3-methyl-6-(1-methyl-1H-pyrrol-2-yl)-1-phenyl-1H-pyrazolo[3,4-b]pyridine-5-carbonitrile (12a). Light brown solid; M.p: 127–129 °C; FT-IR (KBr): ν (cm⁻¹) = 3414, 3114, 3062, 2971, 2930, 2218, 1618, 1596, 1558, 1507, 1486, 1415. ¹H NMR (400 MHz, DMSO-*d*₆) δ 11.94 (s, 1H), 8.19–8.11 (m, 2H), 7.96 (s, 1H), 7.60 (t, *J* = 8.0 Hz, 3H), 7.42 (dd, *J* = 16.1, 7.7 Hz, 2H), 7.24 (t, *J* = 7.2 Hz, 1H), 7.17–7.10 (m, 2H), 6.99 (dd, *J* = 3.9, 1.7 Hz, 1H), 6.21 (dd, *J* = 3.9, 2.6 Hz, 1H), 3.96 (s, 3H), 2.07 (s, 3H). ¹³C NMR (101 MHz, DMSO-*d*₆) δ 152.4, 149.5, 147.2, 144.2, 138.1, 135.9, 129.2, 128.2, 127.6, 126.5, 126.2, 122.1, 121.3, 120.2, 119.2, 118.6, 115.3, 113.0, 112.2, 107.9, 107.5, 101.3, 36.35, 14.3, (See SI, Figs. S33–S35).

3-Methyl-6-(1-methyl-1H-pyrrol-2-yl)-4-(4-nitrophenyl)-1-phenyl-1H-pyrazolo[3,4-b]pyridine-5-carbonitrile (13a). Brown solid; M.p: 179–181 °C; FT-IR (KBr): ν (cm⁻¹) = 3071, 2952, 2220, 1598, 1567, 1557, 1507, 1439, 1415. ¹H NMR (400 MHz, DMSO-*d*₆) δ 8.49 (d, *J* = 8.3 Hz, 1H), 8.13 (t, *J* = 7.7 Hz, 3H), 7.98 (d, *J* = 8.1 Hz, 1H), 7.61 (s, 2H), 7.43–7.37 (m, 2H), 7.15 (s, 1H), 7.05–7.01 (m, 1H), 6.23 (s, 1H), 3.95 (s, 3H), 2.02 (s, 3H). ¹³C NMR (101 MHz, DMSO-*d*₆) δ 151.8, 150.3, 149.1, 148.3, 143.6, 140.1, 138.0, 130.6, 130.3, 129.3, 129.2, 128.8, 126.7, 124.9, 123.6, 122.5, 121.34, 119.8, 117.5, 115.6, 107.8, 36.5, 14.3, (See SI, Figs. S36–S38).

3-Methyl-6-(1-methyl-1H-pyrrol-2-yl)-4-(3-nitrophenyl)-1-phenyl-1H-pyrazolo[3,4-b]pyridine-5-carbonitrile (14a). Yellow solid; M.p: 204–206 °C; FT-IR (KBr): ν (cm⁻¹) = 3078, 2955, 2925, 2857, 2214, 1669, 1567, 1535, 1489, 1419. ¹H NMR (600 MHz, DMSO-*d*₆) δ 8.60 (s, 1H), 8.52–8.49 (m, 1H), 8.16 (d, *J* = 7.6 Hz, 1H), 8.13 (d, *J* = 7.7 Hz, 2H), 7.96 (t, *J* = 8.0 Hz, 1H), 7.62 (t, *J* = 7.9 Hz, 2H), 7.41 (t, *J* = 7.4 Hz, 1H), 7.15 (s, 1H), 7.03 (dd, *J* = 3.8, 1.5 Hz, 1H), 6.23 (dd, *J* = 3.7, 2.7 Hz, 1H), 3.95 (s, 3H), 2.03 (s, 3H). ¹³C NMR (151 MHz, DMSO-*d*₆) δ 152.4, 151.9, 149.7, 144.2, 138.5, 135.3, 133.0, 131.4, 129.7, 129.1, 129.1, 128.5, 127.1, 121.8, 118.2, 116.0, 112.4, 108.2, 100.9, 36.9, 14.8, (See SI, Figs. S39–S41).

4-(5-Cyano-3-methyl-6-(1-methyl-1H-pyrrol-2-yl)-1-phenyl-1H-pyrazolo[3,4-b]pyridin-4-yl)benzoic acid (15a). Beige solid; M.p: 177–179 °C; FT-IR (KBr): ν (cm⁻¹) = 3420, 3107, 2971, 2931, 2217, 1709, 1666, 1599, 1556, 1508, 1439, 1419. ¹H NMR (400 MHz, DMSO-*d*₆) δ 8.14–8.11 (m, 4H), 7.66 (d, *J* = 8.1 Hz, 2H), 7.61 (t, *J* = 7.9 Hz, 2H), 7.40 (t, *J* = 7.4 Hz, 1H), 7.15–7.11 (m, 1H), 7.01 (dd, *J* = 3.9, 1.6 Hz, 1H), 6.22 (dd, *J* = 3.8, 2.6 Hz, 1H), 3.95 (s, 3H), 2.03 (s, 3H). ¹³C NMR (101 MHz, DMSO-*d*₆) δ 167.8, 152.9, 152.4, 149.7, 144.3, 138.5, 136.4, 129.7, 129.6, 129.1, 128.6, 127.1, 121.8, 118.2, 116.0, 112.3, 108.2, 100.7, 36.9, 14.7, (See SI, Figs. S42–S44).

4,4'-(1,4-Phenylene)bis(3-methyl-6-(1-methyl-1H-pyrrol-2-yl)-1-phenyl-1H-pyrazolo[3,4-b]pyridine-5-carbonitrile (16a). Beige solid; dec.: 320 °C; FT-IR (KBr): ν (cm⁻¹) = 3064, 2949, 2220, 1646, 1566, 1507, 1436, 1417. ¹H NMR (400 MHz, DMSO-*d*₆) δ ¹H NMR (400 MHz, DMSO) δ 8.16 (d, *J* = 8.4 Hz, 4H), 7.93 (d, *J* = 8.7 Hz, 3H), 7.66–7.58 (m, 5H), 7.41 (d, *J* = 7.0 Hz, 2H), 7.16 (s, 2H), 7.07 (dd, *J* = 3.7, 1.4 Hz, 2H), 6.27–6.23 (m, 2H), 3.98 (s, 6H), 2.15 (s, 3H), 2.12 (s, 3H), (See SI, Figs. S45–S46).

4,4'-(1,3-Phenylene)bis(3-methyl-6-(1-methyl-1H-pyrrol-2-yl)-1-phenyl-1H-pyrazolo[3,4-b]pyridine-5-carbonitrile (17a)ss. Brown solid; M.p: 248–250 °C; FT-IR (KBr): ν (cm⁻¹) = 3463, 2950, 2220, 1660, 1599, 1570, 1558, 1506, 1490, 1416. ¹H NMR (400 MHz, DMSO-*d*₆) δ 8.13 (d, *J* = 7.8 Hz, 4H), 7.91 (d, *J* = 7.9 Hz, 2H), 7.63–7.59 (m, 5H), 7.40 (t, *J* = 7.4 Hz, 3H), 7.14 (d, *J* = 1.9 Hz, 2H), 7.01 (dd, *J* = 3.9, 1.6 Hz, 2H), 6.22 (dd, *J* = 3.7, 2.7 Hz, 2H), 3.96 (s, 6H), 2.13 (s, 6H). ¹³C NMR (101 MHz, DMSO-*d*₆) δ 151.8, 151.8, 149.1, 144.0, 138.0, 134.4, 129.9, 129.3, 129.0, 128.7, 128.5, 128.0, 126.6, 121.3, 117.7, 115.5, 112.1, 107.7, 100.6, 36.5, 14.0, (See SI, Figs. S47–S49).

4,4',4''-(((1,3,5-Triazine-2,4,6-triyl)tris(oxy))tris(benzene-4,1-diyl))tris(3-methyl-6-(1-methyl-1H-pyrrol-2-yl)-1-phenyl-1H-pyrazolo[3,4-b]pyridine-5-carbonitrile (18a)s. Brown solid; M.p: 131–133 °C; FT-IR (KBr): ν (cm⁻¹) = 3118, 2928, 2877, 2806, 2217, 1662, 1612, 1593, 1561, 1516, 1487, 1439. ¹H NMR (400 MHz, DMSO-*d*₆) δ 8.15–8.09 (m, 6H), 7.60 (dd, *J* = 10.9, 5.1 Hz, 6H), 7.46 (d, *J* = 8.6 Hz, 6H), 7.39 (t, *J* = 7.4 Hz, 3H), 7.13–7.10 (m, 3H), 7.00 (d, *J* = 1.8 Hz, 3H), 6.98 (dd, *J* = 3.3, 2.1 Hz, 6H), 6.21 (dd, *J* = 3.9, 2.6 Hz, 3H), 3.93 (s, 9H), 2.11 (s, 9H). ¹³C NMR (101 MHz, DMSO-*d*₆) δ 162.2, 159.1, 153.2, 152.0, 149.3, 144.0, 138.1, 130.7, 129.2, 129.0, 128.3, 128.2, 126.4, 123.8, 123.2, 121.2, 118.1, 115.4, 115.2, 112.2, 107.6, 100.5, 30.5, 14.4, (See SI, Figs. S50–S52).

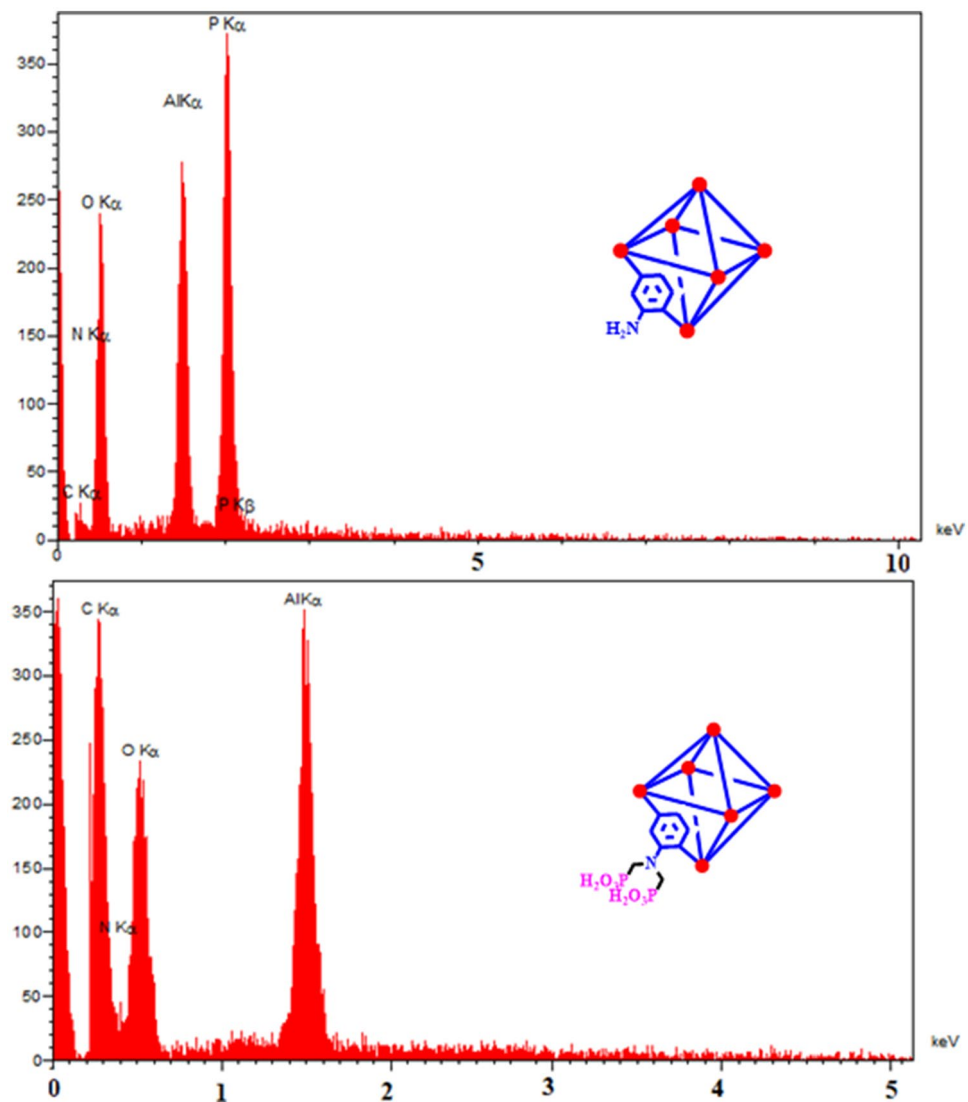


Figure 9. EDX analysis and elemental mapping of electro-synthesized MIL-53(Al)-NH₂ and MIL-53(Al)-N(CH₂PO₃H₂)₂.

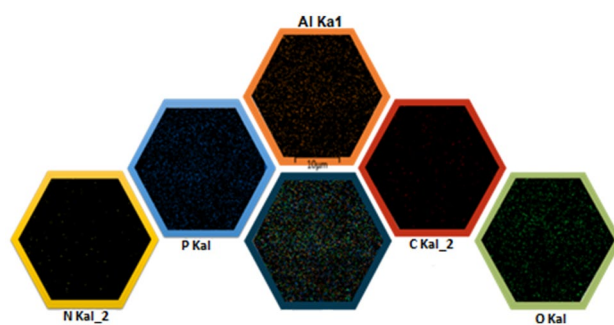


Figure 10. Elemental maps (EDX) of C (red); N (yellow); Al (orange); P (blue) and O (green) atoms for MIL-53(Al)-N(CH₂PO₃H₂)₂.

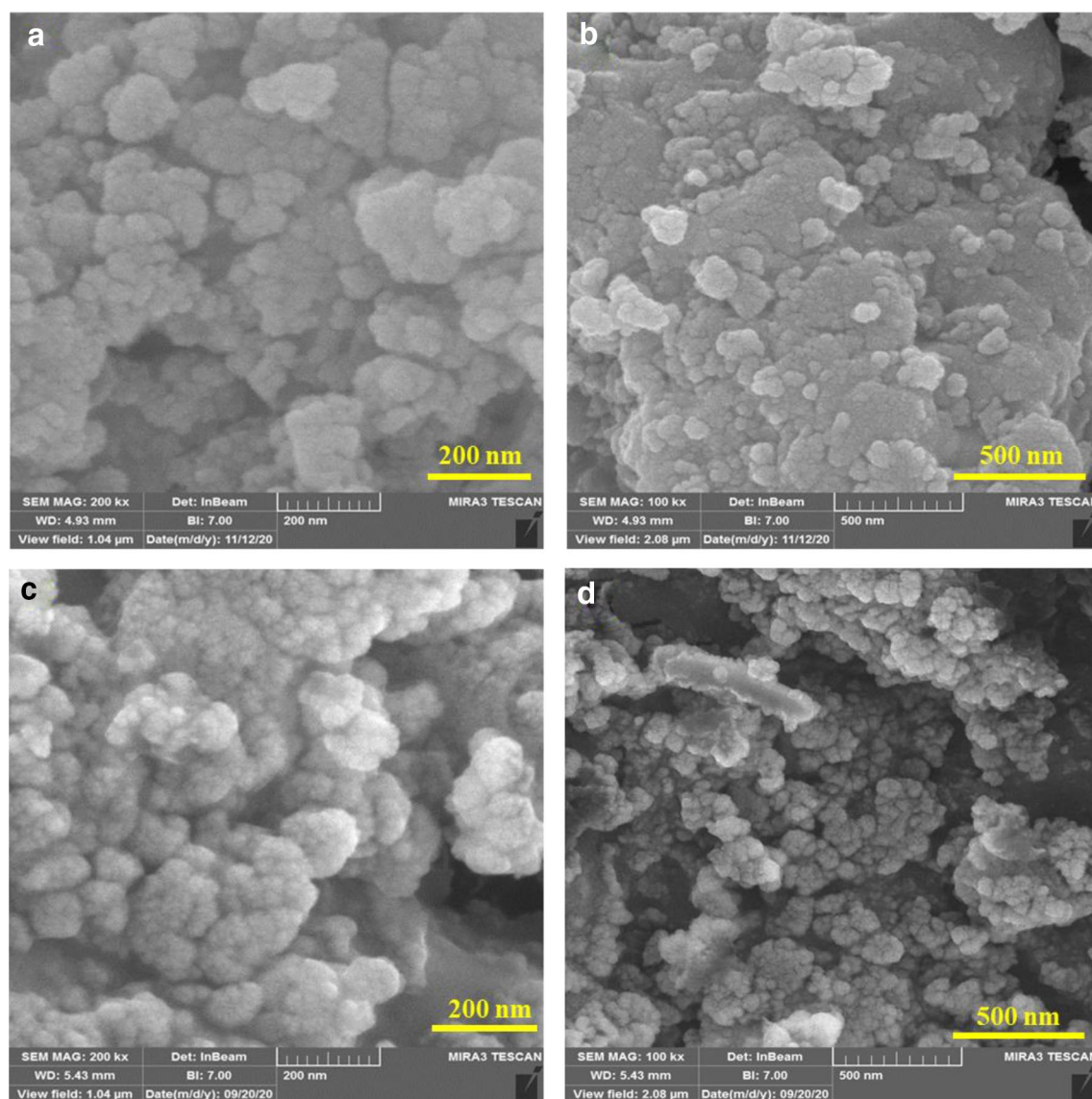


Figure 11. FE-SEM images of MIL-53(Al)-NH₂ (a,b) and MIL-53(Al)-N(CH₂PO₃H₂)₂ (c,d).

Results and discussion

In order to develop the catalytic application of metal–organic frameworks (MOFs), MIL-53(Al)-NH₂ was prepared by anodic electrosynthesis technique (Fig. 6). Post-functionalization of MIL-53(Al)-NH₂ for preparing of MIL-53(Al)-N(CH₂PO₃H₂)₂ was occurred by using paraformaldehyde under refluxing ethanol and presence *p*-TSA. To shed light of this issue, at the first step, we employed an anodic electrosynthesis procedure for the preparation of MIL-53(Al)-NH₂. This mode has accomplished by inserting two aluminium metallic plates in the presence of H₂BDC-NH₂ and KNO₃ as ligand and supporting electrolyte, respectively at room temperature in an EtOH/H₂O (10/90, v/v) mixture under stirring. Aluminium metal plays the role of cation source and also the anodic and cathodic electrodes. Upon the establishment of the current density (10.0 mA cm⁻² at 30 min), the increased pH at the cathode surface thanks to the in-situ electrogeneration of hydroxide ions makes deprotonation of ligands by electroreduction of water molecules. On the other hand, the anode surface starts to oxidize in order to the preparation of aluminium cations to coordinate with the available ligands. The activated ligands can be coordinated to the available cations to starting the crystallinity of MIL-53(Al)-NH₂ (Fig. 6). This process has some advantages as in-situ deprotonation of ligand, in-situ cation electrogeneration, cation-controlled release, and avoiding of the pore-blocking due to the absence of the related cation salt. The MIL-53(Al)-NH₂ has prepared without the need of any ex-situ base/probase and cation salt additive, at room temperature, atmospheric pressure, and short reaction time. At the second step, the post-modification of the prepared MIL-53(Al)-NH₂ with the phosphorous acid tags was performed in the percent of *p*-TSA and paraformaldehyde under refluxing ethanol. To shed light of the more details, the full characterization of the MIL-53(Al)-NH₂ and MIL-53(Al)-N(CH₂PO₃H₂)₂ as a porous material catalyst was evaluated by FT-IR, X-ray diffraction analysis (XRD), energy-dispersive X-ray spectroscopy (EDX), FE-SEM, elemental mapping, thermal gravimetric (TG) and derivative thermal gravimetric (DTG) techniques.

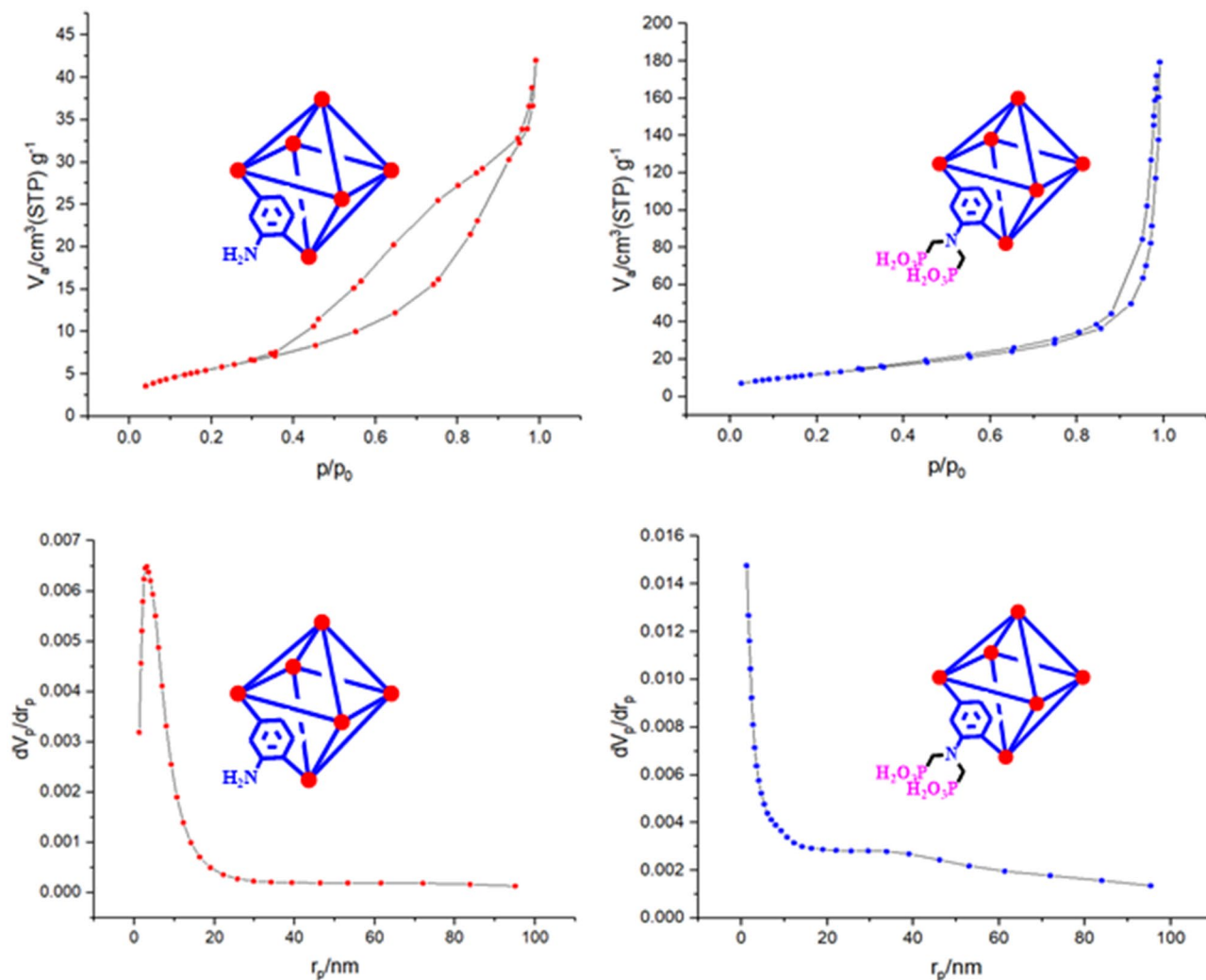


Figure 12. N_2 adsorption/desorption isotherm and BJH of MIL-53(Al)- $N(CH_2PO_3H_2)_2$ and MIL-53(Al)- $N(CH_2PO_3H_2)_2$.

The FT-IR analysis was surveyed for verification of the functional groups and bonding properties in the synthesized MOF as a catalyst. The FT-IR spectra of 2-amino terephthalic acid as susceptible ligand, phosphorus acid, MIL-53(Al)- NH_2 and MIL-53(Al)- $N(CH_2PO_3H_2)_2$ MOFs were shown in Fig. 7. The broad peak $2600\text{--}3500\text{ cm}^{-1}$ is related to the OH of PO_3H_2 functional groups. Also, the absence of the OH groups' (carboxylic acid) peak $2488\text{--}3500\text{ cm}^{-1}$ in the ligand spectrum. Then, the absence of free C=O functional groups shifting of the characteristic couple bands from 1689 cm^{-1} in the ligand spectrum to the 1672 cm^{-1} in the MOFs spectra can be assigned to the coordination of the COO^- groups with the aluminium metallic cations. Besides, the presence of the two sharp bands at 3485 and 3387 cm^{-1} in the MIL-53(Al)- NH_2 spectrum indicates the symmetric and asymmetric vibrations of the NH_2 groups^{35–37,72–78}. The absorption bands at 944 and 1015 cm^{-1} are related to P-O bond stretching and the band at 1132 cm^{-1} is related to P=O. The FT-IR spectrum difference between MIL-53(Al)- NH_2 and MIL-53(Al)- $N(CH_2PO_3H_2)_2$ verified the structure of the desired post-synthesized catalyst.

To study the purity and crystallinity of the synthesized MOF structures, the XRD patterns were recorded. According to the XRD profile (Fig. 8), the MIL-53(Al)- NH_2 and MIL-53(Al)- $N(CH_2PO_3H_2)_2$ are isoreticular materials with suitable crystallinity and without any impurity or contaminants. Comparing the three characteristic peaks located at the $2\theta = 9.27^\circ$, 12.40° , and 17.50° , 25.10° with previously reported data is approved their structures^{35–37,72–78}.

For more details, the EDX analysis was also accomplished for elemental analysis and elemental dispersity of prepared MOFs (Fig. 9). The emerged elemental peaks approved the existence of C, O, N, and Al elements in the MIL-53(Al)- NH_2 structure and P element in the MIL-53(Al)- $N(CH_2PO_3H_2)_2$ structure. Besides, the EDX mapping images indicates the uniform and homogeneous distribution of elements (Fig. 10).

Also, FE-SEM images of electro-synthesized MIL-53(Al)- NH_2 and its post-functionalized one were recorded for investigation of their morphologies (Fig. 11). The obtained images exhibit the uniform cauliflower-shaped nanoparticles with an average diameter size of around 33.0 nm . The increasing of the EtOH/ H_2O ratio than pure H_2O solvent in the electrosynthesis procedure can lead to the lower crystallinity of structure and smaller particles^{32–34}.

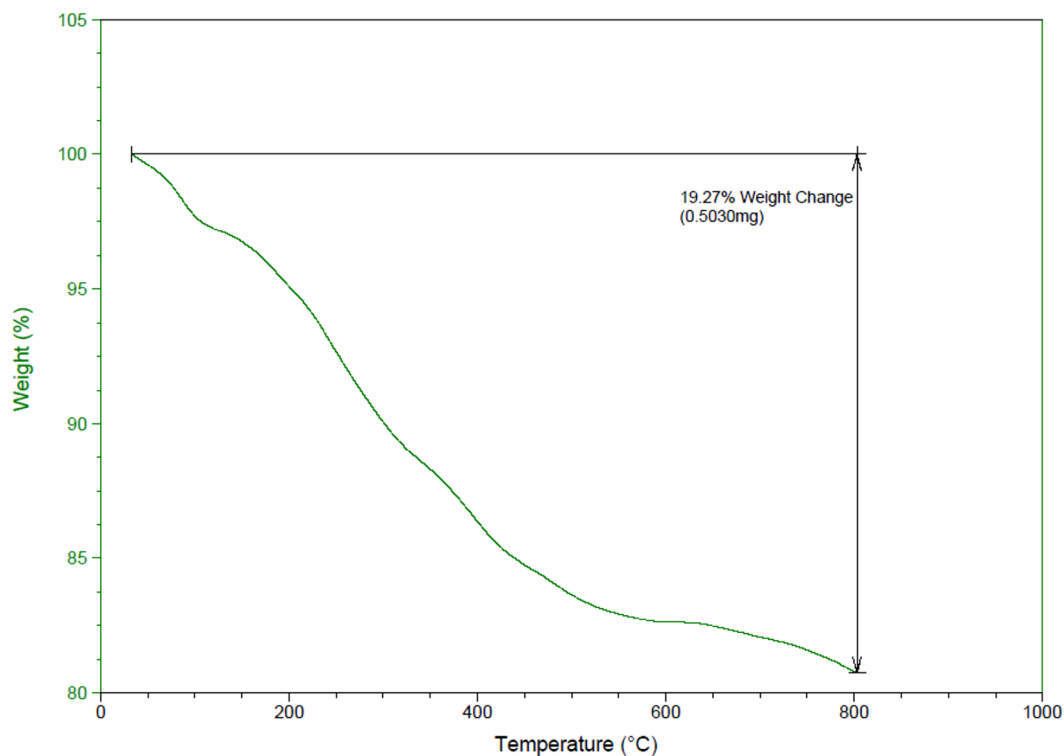


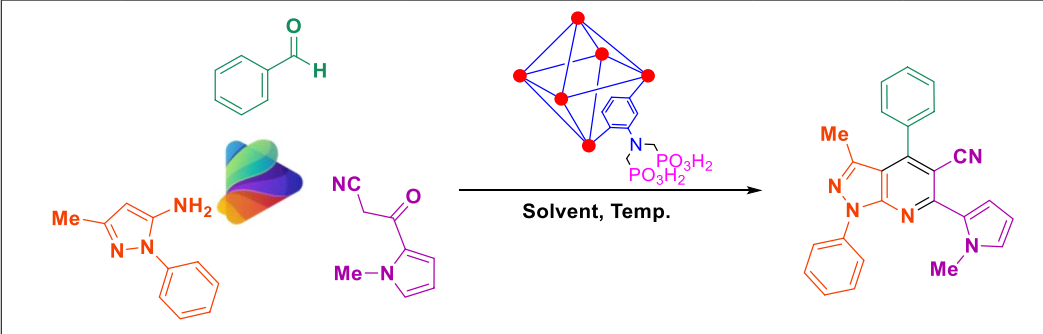
Figure 13. Thermogravimetric (TGA) analysis of MIL-53(Al)-N(CH₂PO₃H₂)₂.

The specific surface area and pore size distribution are considered as significant parameters of the prepared porous materials and can be affected on the catalysis performance. In this way, the N₂ adsorption/desorption technique was employed for the investigation of the MIL-53(Al)-NH₂ and MIL-53(Al)-N(CH₂PO₃H₂)₂ structure porosity (Fig. 12). As can be seen, the N₂ adsorption/desorption plots exhibit the IV-type isotherms with the hysteresis loops as a feature of the mesoporous materials. It is noteworthy, the created mesophase is consistent with the fact that increased EtOH/H₂O ratio in the synthesis process can lead to mesoporosity structures^{32–34}. According to the obtained BET results, the specific surface areas of MIL-53(Al)-NH₂ and MIL-53(Al)-N(CH₂PO₃H₂)₂ structure are 204.75 and 132.19 m² g⁻¹, respectively. Also, according to the obtained BJH information, the pore size of MIL-53(Al)-NH₂ and MIL-53(Al)-N(CH₂PO₃H₂)₂ structure was determined to be 4.2 nm and 3.2 nm, respectively. It should be noted that the surface area and pore size of functionalized MOF was decreased. Thus, it can be assigned to the presence of the larger phosphorus acid tags than amine groups during the post-modification process.

The thermogravimetric (TGA) analysis for MIL-53(Al)-N(CH₂PO₃H₂)₂ was performed to study at range of 50–800 °C, with a temperature increase rate of 10 °C min⁻¹ in CO₂ atmosphere (Fig. 13). The first distinguished weight loss step in the temperature zone of 50–100 °C can be assigned to the evaporation and removal of solvents. The second distinguished weight loss step in the temperature zone of 150–450 °C can be assigned to the decomposition of the organic section of material includes the ligand and phosphorus acid which leads to the degradation and collapse of the framework.

After identification of MIL-53(Al)-N(CH₂PO₃H₂)₂ as mesoporous hybrid-catalyst, we tested its catalytic activity in the preparation of novel organic and biological interest candidates (*N*-methyl-pyrrol)-pyrazolo[3,4-*b*]pyridines derivatives. Optimization of reaction for synthesis of target molecules were done by one-pot reaction of benzaldehyde (1.0 mmol, 0.106 g), 3-methyl-1-phenyl-1*H*-pyrazol-5-amine (1.0 mmol, 0.174 g) and 3-(1-methyl-1*H*-pyrrol-2-yl)-3-oxopropanenitrile (1.0 mmol, 0.148 g) as a model reaction. The optimized data is listed in Table 1. As shown, the most optimal one-pot reaction for the preparation of (*N*-methyl-pyrrol)-pyrazolo[3,4-*b*]pyridines is reported in the presence of 10.0 mg MIL-53(Al)-N(CH₂PO₃H₂)₂ at 110 °C under solvent-free condition (Table 1 entry 4). The obtained data for the model reaction using other amounts of catalyst and temperature shows that the yield and time were not improved (Table 1 entries 1–8 except 4). The model reaction was also studied by using several solvents such as EtOH, CH₂Cl₂, CHCl₃, EtOAc, CH₃CN, PEG, *n*-Hexane, H₂O and DMF (5.0 mL) and solvent-free condition in the presence of 10.0 mg of catalyst. The results of the reaction did not improve (Table 1, entries 9–17).

After optimizing the reaction conditions, MIL-53(Al)-N(CH₂PO₃H₂)₂ (10.0 mg) is applied to synthesis a good range of new biological and pharmacological interest candidates using various aromatic aldehyde derivatives (trephetaldehyde, iso-trephetaldehyde, tripod-aldehyde, heterocycle, bearing electron-donating and electron-withdrawing groups), 3-methyl-1-phenyl-1*H*-pyrazol-5-amine and 3-(1-methyl-1*H*-pyrrol-2-yl)-3-oxopropanenitrile. As shown in Tables 2 and 3, the obtained results indicated that MIL-53(Al)-N(CH₂PO₃H₂)₂ is



Entry	Amount of cat. (mg)	Temp. (°C)	Time (min)	Solvent	Yield ^a (%)
1	–	110	60	–	Trace
2	5	110	60	–	35
3	7.5	110	60	–	55
4	10	110	25	–	88
5	15	110	25	–	88
6	10	75	60	–	65
7	10	50	60	–	40
8	10	r.t	60	–	Trace
9	10	Reflux	60	EtOH	52
10	10	Reflux	60	CH ₂ Cl ₂	Trace
11	10	Reflux	60	CHCl ₃	45
12	10	Reflux	60	EtOAc	48
13	10	Reflux	60	CH ₃ CN	55
14	10	110	60	PEG	65
15	10	Reflux	60	<i>n</i> -Hexane	Trace
16	10	Reflux	60	H ₂ O	45
17	10	110	60	DMF	55

Table 1. Effect of different amounts of catalysts, temperature and solvent (5 mL) in the synthesis of (*N*-methyl-pyrrol)-pyrazolo[3,4-*b*]pyridines. ^aReaction conditions: benzaldehyde (1.0 mmol, 0.106 g), 3-methyl-1-phenyl-1*H*-pyrazol-5-amine (1.0 mmol, 0.174 g) and 3-(1-methyl-1*H*-pyrrol-2-yl)-3-oxopropanenitrile (1.0 mmol, 0.148 g).

appropriate for the preparation of target molecules in high to excellent yields (65–92%) within relatively short reaction times (20–40 min). Interestingly, when we synthesized (*N*-methyl-pyrrol)-pyrazolo[3,4-*b*]pyridines in the percent indole aldehyde as a biological and pharmacological compound (Table 2). Also, the preparation of bis and tris-(*N*-methyl-pyrrol)-pyrazolo[3,4-*b*]pyridines by the condensation of 3-methyl-1-phenyl-1*H*-pyrazol-5-amine and 3-(1-methyl-1*H*-pyrrol-2-yl)-3-oxopropanenitrile with terephthalaldehyde, *iso*-terephthalaldehyde and tripodal aldehyde using MIL-53(Al)-N(CH₂PO₃H₂)₂ (10.0 mg) at 110 °C under solvent-free condition (Table 3).

In suggested mechanism, aldehyde is activated with PO₃H₂ tags of MIL-53(Al)-N(CH₂PO₃H₂)₂ and intermediate (I) is prepared by reaction of 3-(1-methyl-1*H*-pyrrol-2-yl)-3-oxopropanenitrile with the loss of H₂O. In the second step, phenyl pyrazol-5-amine react with intermediate (I) to gives intermediate (II) after tautomerization. Then, intermediate (II) gives intermediates (III) after intramolecular cyclization and loss of one molecule of H₂O. Then, the corresponding product (IV) is produced via a cooperative vinylogous anomeric based oxidation mechanism both in the presence and absence of oxygen (pathways A and B in Fig. 14)^{62,63,67,68,79}. It should be mentioned that the reaction in the absence of oxygen and under both nitrogen and argon atmospheres have proceeded as same as in the presence of oxygen. Recently, we have comprehensively showed that the hetero atoms have stereoelectronic effects of common origin and that anomeric effect is one of them⁸⁰.

To evaluate the performance of MIL-53(Al)-N(CH₂PO₃H₂)₂ as a catalyst for the synthesis of (*N*-methyl-pyrrol)-pyrazolo[3,4-*b*]pyridines, we have tested various acid catalysts (organic and inorganic) in the reaction of benzaldehyde (1.0 mmol, 0.106 g), 3-methyl-1-phenyl-1*H*-pyrazol-5-amine (1.0 mmol, 0.174 g) and 3-(1-methyl-1*H*-pyrrol-2-yl)-3-oxopropanenitrile (1.0 mmol, 0.148 g) in Table 4. The obtained results which are collected in Table 4 shows that, MIL-53(Al)-N(CH₂PO₃H₂)₂ is the best catalyst for the synthesis of a novel (*N*-methyl-pyrrol)-pyrazolo[3,4-*b*]pyridines.

The obtained results of catalytic activity and reusability of MIL-53(Al)-N(CH₂PO₃H₂)₂ were added in (Fig. 15). As above said, MIL-53(Al)-N(CH₂PO₃H₂)₂ was separated by centrifugation and reused without significantly reducing its catalytic activity. For this purpose, recyclability of the catalyst was also studied on the one-pot reaction of benzaldehyde (1.0 mmol, 0.106 g), 3-methyl-1-phenyl-1*H*-pyrazol-5-amine (1.0 mmol, 0.174 g) and 3-(1-methyl-1*H*-pyrrol-2-yl)-3-oxopropanenitrile (1.0 mmol, 0.148 g) as a model reaction under

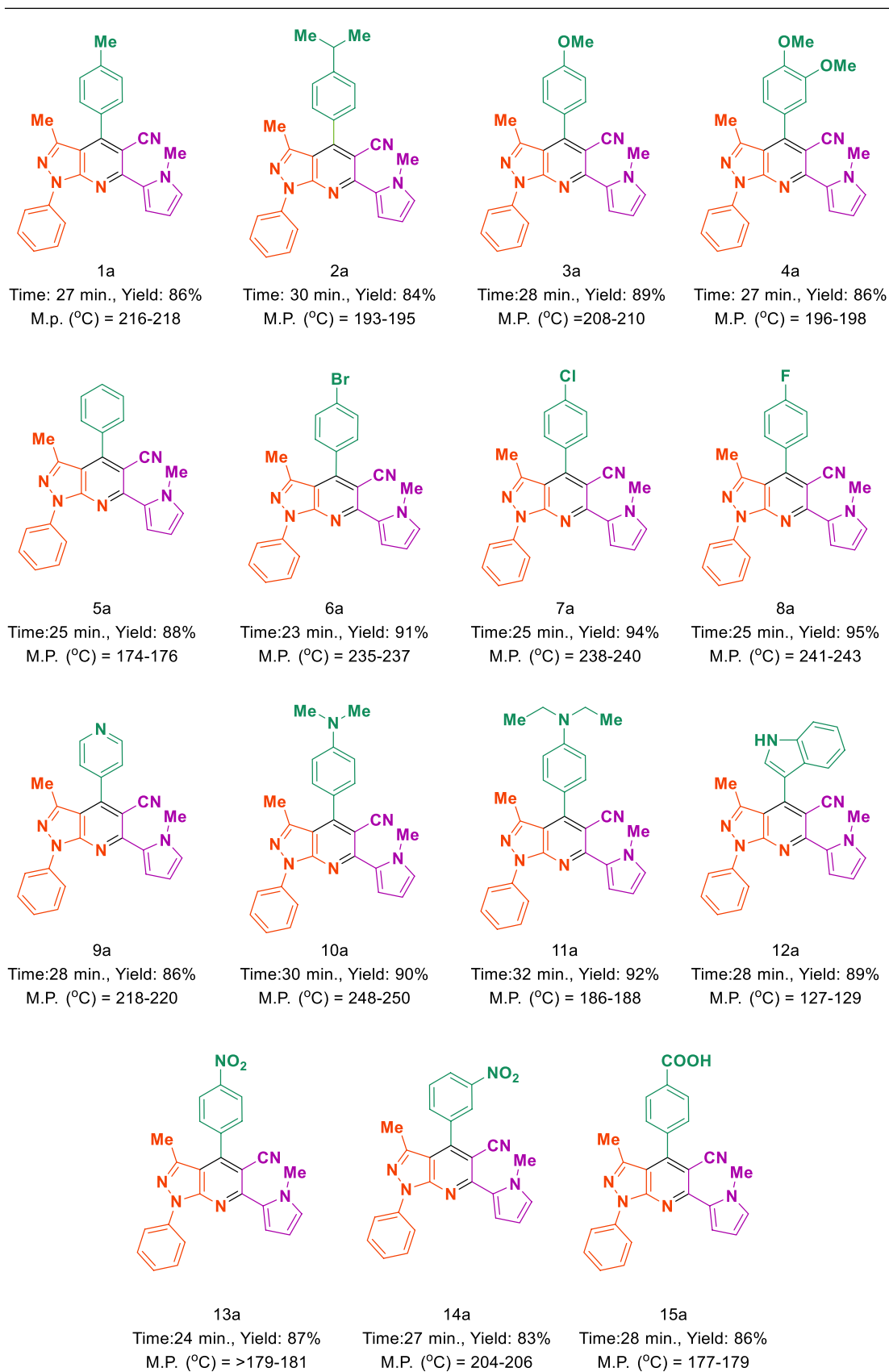


Table 2. Synthesis of (*N*-methyl-pyrrol)-pyrazolo[3,4-*b*]pyridines using MIL-53(Al)- $N(\text{CH}_2\text{PO}_3\text{H}_2)_2$ (10 mg) at 110 °C under solvent-free condition.

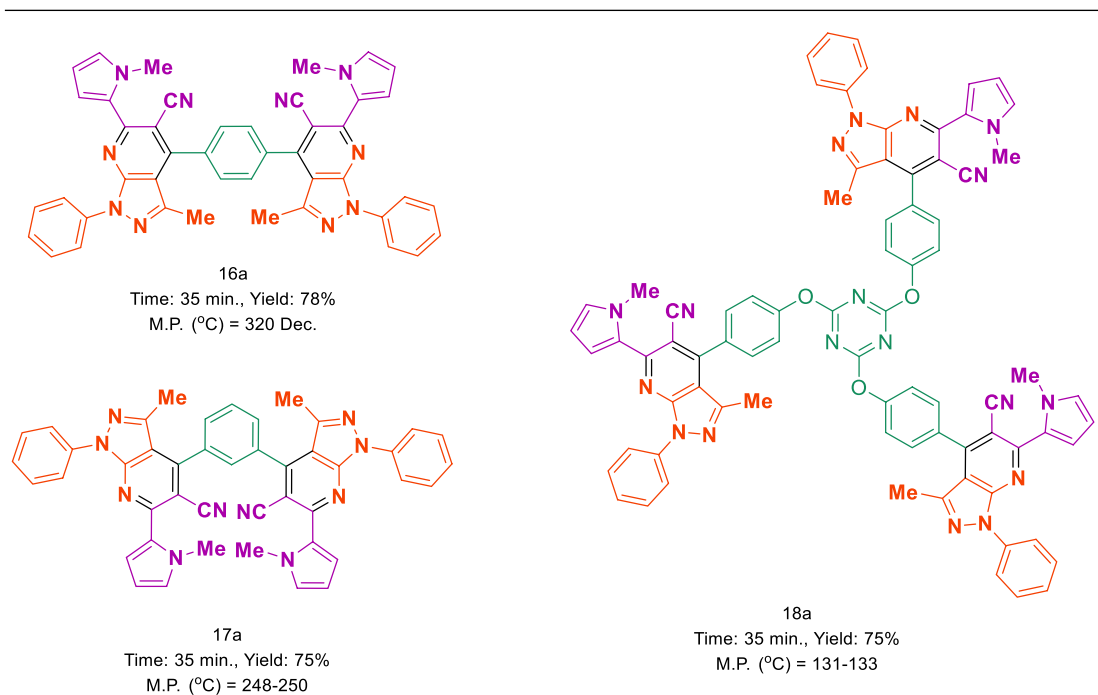


Table 3. Synthesis of (*N*-methyl-pyrrol)-pyrazolo[3,4-*b*]pyridines using MIL-53(Al)-N(CH₂PO₃H₂)₂ (10 mg) at 110 °C under solvent-free condition.

the above-mentioned optimized reaction conditions. Therefore, MIL-53(Al)-N(CH₂PO₃H₂)₂ can be reused up to five times without noticeable changes in its catalytic activity.

The large scale synthesis of (*N*-methyl-pyrrol)-pyrazolo[3,4-*b*]pyridines by the reaction of aldehyde (20 mmol), 3-methyl-1-phenyl-1*H*-pyrazol-5-amine (20 mmol, 3.48 g) and 3-(1-methyl-1*H*-pyrrol-2-yl)-3-oxopropanenitrile (20 mmol, 2.96 g) using MIL-53(Al)-N(CH₂PO₃H₂)₂ (1 g) at 110 °C (Table 5).

Conclusion

In this study, electrosynthesis of MIL-53(Al)-NH₂ as a metal–organic framework was presented. The anodic electrosynthesis as an environmentally friendly technique procedure was performed in the aqueous solution, room temperature, and atmospheric pressure in the shortest possible time. Also, the employed electrochemical technique provided a promising procedure for the preparation of mesoporous catalyst with a shorter time and high yield. Then its functionalization with the phosphorus acid tags through the post-modification process has occurred. It is noteworthy, this procedure was accomplished without the need for the ex-situ salt and base/pre-base additives as cation source and ligand activating agent, respectively. MIL-53(Al)-N(CH₂PO₃H₂)₂ as an efficient catalyst was used for the synthesis of the novel (*N*-methyl-pyrrol)-pyrazolo[3,4-*b*]pyridines as biological interest molecules via a cooperative vinylogous anomeric based oxidation mechanism. Short reaction time, clean profile of reaction, recycling and reusing of catalyst are the major advantages of the presented work. We think that the present work can open up a promising insight for developing of anomeric effect in the course of organic synthesis.

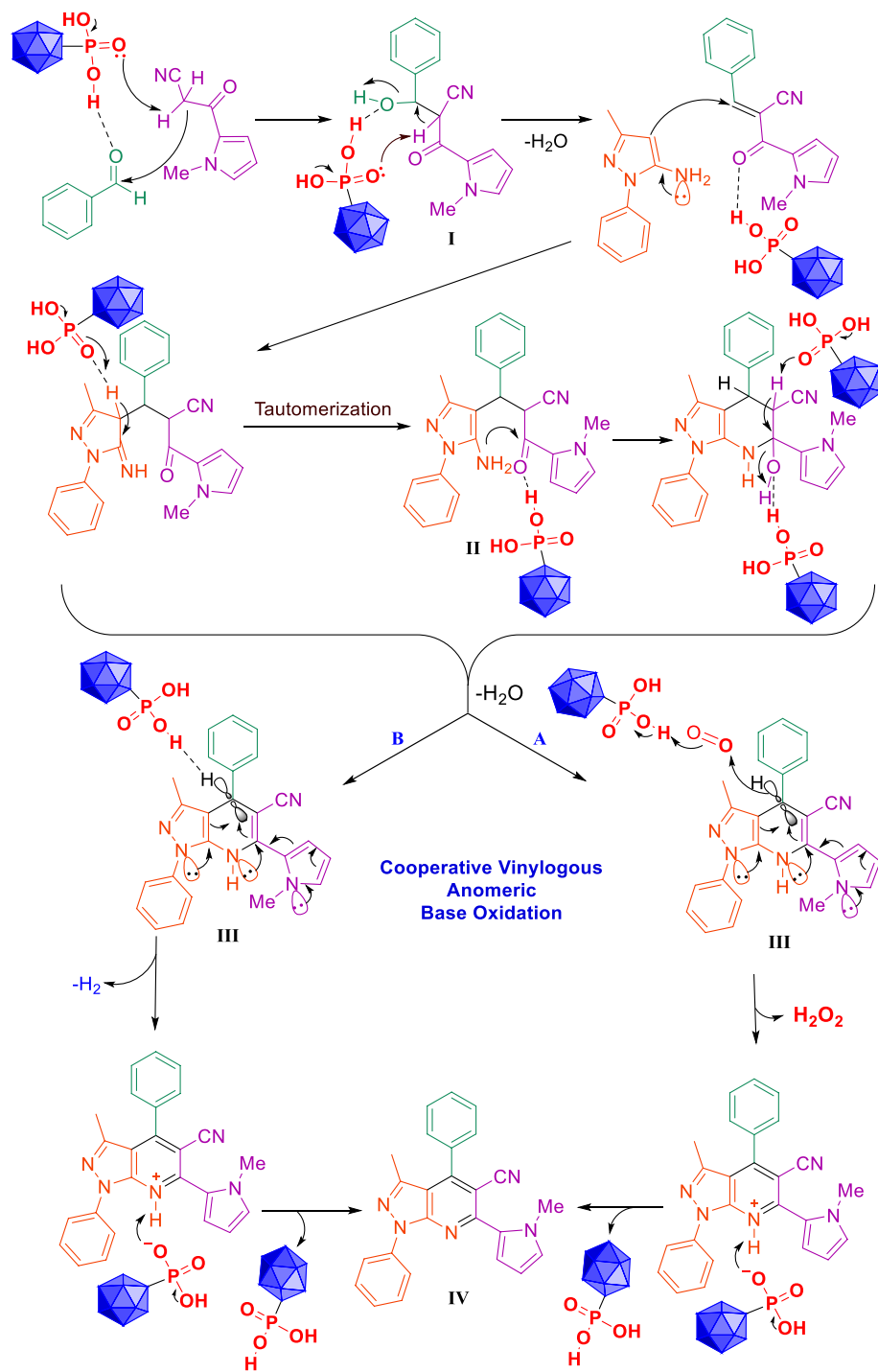
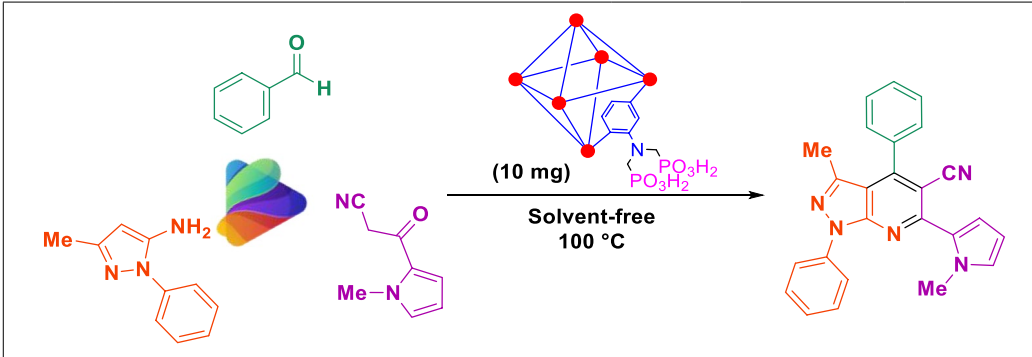


Figure 14. Plausible mechanisms for the synthesis (N-methyl-pyrrol)-pyrazolo[3,4-b]pyridines using MIL-53(Al)-N(CH₂PO₃H₂)₂.



Entry	Catalyst	(mg)	Time (min)	Yield (%)
1	[PVI-SO ₃ H]FeCl ₄ ⁸¹	10	60	55
2	NaHSO ₄	10 mol%	60	28
3	Fe ₂ O ₄	10	60	35
4	SSA ⁸²	10	60	45
5	[Fe ₃ O ₄ @SiO ₂ @(CH ₂) ₃ -DABCO-SO ₃ H]Cl ₂ ⁸³	10	60	35
6	FeCl ₃	10 mol%	60	45
7	TrBr ⁸⁴	10 mol%	60	Trace
8	GTBSA ⁸⁵	10 mol%	60	65
9	Mg(NO ₃) ₂ ·6H ₂ O	10 mol%	60	Trace
10	[Py-SO ₃ H]Cl ⁸⁶	10 mol%	60	65
11	NH ₄ NO ₃	10 mol%	60	–
12	MIL-100(Cr)/NHEtN(CH ₂ PO ₃ H ₂) ₂ ⁴⁷	10	60	75
13	APVPB ⁸⁷	10	60	45
14	MHMHPA ⁵⁰	10 mol%	60	55
15	MIL-53(Al)-N(CH ₂ PO ₃ H ₂) ₂ ^{This work}	10	25	88

Table 4. Evaluation of various catalyst for the synthesis of novel (*N*-methyl-pyrrol)-pyrazolo[3,4-*b*]pyridines in comparison with MIL-53(Al)-N(CH₂PO₃H₂)₂.

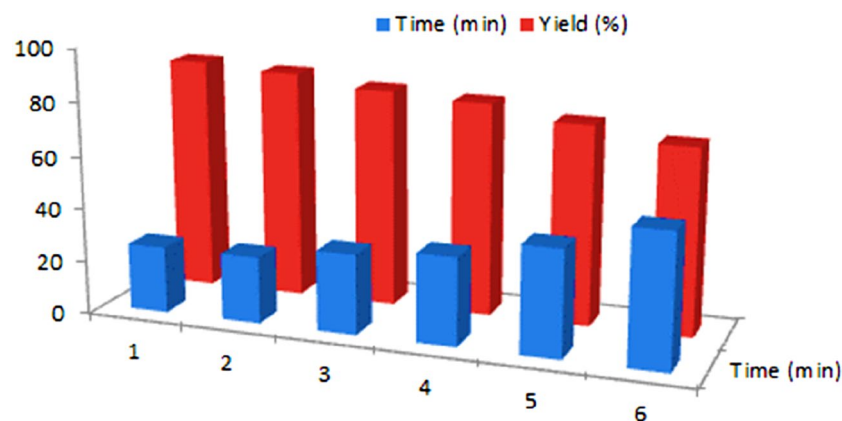


Figure 15. Reusability of MIL-53(Al)-N(CH₂PO₃H₂)₂.

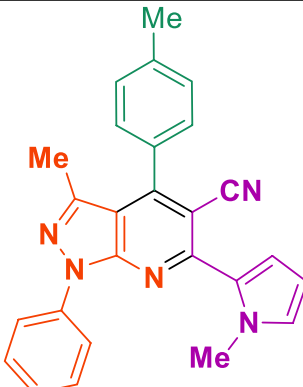
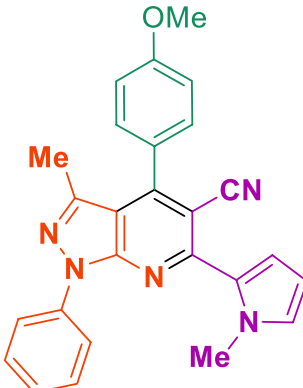
Entry	Product	Time (min)	Yield (%)	M.p. °C
1		55	75	216–218
2		60	65	209–211

Table 5. Large scale synthesis of (*N*-methyl-pyrrol)-pyrazolo[3,4-*b*]pyridines.

Received: 4 May 2021; Accepted: 24 August 2021
Published online: 29 September 2021

References

- Furukawa, H., Cordova, K. E., O’Keeffe, M. & Yaghi, O. M. The chemistry and applications of metal-organic frameworks. *Science* **341**, 1230444 (2013).
- Long, J. R. & Yaghi, O. M. The pervasive chemistry of metal-organic frameworks. *Chem. Soc. Rev.* **38**, 1213–1214 (2009).
- Sumida, K. *et al.* Sol-gel processing of metal-organic frameworks. *Chem. Mater.* **29**, 2626–2645 (2017).
- Czaja, A. U., Trukhan, N. & Müller, U. Industrial applications of metal-organic frameworks. *Chem. Soc. Rev.* **38**, 1284–1293 (2009).
- Mueller, U. *et al.* Metal-organic frameworks-prospective industrial applications. *J. Mater. Chem.* **16**, 626–636 (2006).
- Silva, P., Vilela, S. M., Tomé, J. P. & Paz, F. A. A. Multifunctional metal-organic frameworks: from academia to industrial applications. *Chem. Soc. Rev.* **44**, 6774–6803 (2015).
- Liu, L., Zhou, Y., Liu, S. & Xu, M. The applications of metal-organic frameworks in electrochemical sensors. *ChemElectroChem* **5**, 6–19 (2018).
- Sheberla, D. *et al.* Conductive MOF electrodes for stable supercapacitors with high areal capacitance. *Nat. Mater.* **16**, 220–224 (2017).
- Liu, J. & Wöll, C. Surface-supported metal-organic framework thin films: Fabrication methods, applications, and challenges. *Chem. Soc. Rev.* **46**, 5730–5770 (2017).
- Huang, K., Wang, B., Guo, S. & Li, K. Micropatterned ultrathin MOF membranes with enhanced molecular sieving property. *Angew. Chem. Int. Ed.* **57**, 13892–13896 (2018).
- Gu, Z. G., Chen, S. C., Fu, W. Q., Zheng, Q. & Zhang, J. Epitaxial growth of MOF thin film for modifying the dielectric layer in organic field-effect transistors. *ACS Appl. Mater. Interfaces.* **9**, 7259–7264 (2017).
- Ghamari, F., Raoufi, D., Alizadeh, S., Arjomandi, J. & Nematollahi, D. Construction of highly efficient new binder-free bimetallic metal-organic framework symmetric supercapacitors: CONSIDERING surface statistical and morphological analyses. *J. Mater. Chem. A* **9**, 15381–15393 (2021).
- Zhang, X. *et al.* Carbonization of single polyacrylonitrile chains in coordination nanospaces. *Chem. Sci.* **11**, 10844–10849 (2020).
- Mochizuki, S., Kitao, T. & Uemura, T. Controlled polymerizations using metal-organic frameworks. *Chem. Commun.* **54**, 11843–11856 (2018).
- Kong, X. *et al.* Mapping of functional groups in metal-organic frameworks. *Science* **341**, 882–885 (2013).
- Wang, Z. & Cohen, S. M. Postsynthetic modification of metal-organic frameworks. *Chem. Soc. Rev.* **38**, 1315–1329 (2009).
- Stassen, I. *et al.* Electrochemical film deposition of the zirconium metal-organic framework UiO-66 and application in a miniaturized sorbent trap. *Chem. Mater.* **27**, 1801–1807 (2015).
- Li, M. & Dinca, M. Reductive electrosynthesis of crystalline metal-organic frameworks. *J. Am. Chem. Soc.* **133**, 12926–12929 (2011).
- Falcaro, P., Buso, D., Hill, A. J. & Doherty, C. M. Patterning techniques for metal organic frameworks. *Adv. Mater.* **24**, 3153–3168 (2012).

20. Zacher, D., Shekhah, O., Wöll, C. & Fischer, R. A. Thin films of metal–organic frameworks. *Chem. Soc. Rev.* **38**, 1418–1429 (2009).
21. Betard, A. & Fischer, R. A. Metal–organic framework thin films: from fundamentals to applications. *Chem. Rev.* **112**, 1055–1083 (2012).
22. Soury, S., Bahrami, A., Alizadeh, S., Shahna, F. G. & Nematollahi, D. Development of a needle trap device packed with zinc based metal–organic framework sorbent for the sampling and analysis of polycyclic aromatic hydrocarbons in the air. *Microchem. J.* **148**, 346–354 (2019).
23. Firoozichahak, A. *et al.* UIO-66-NH₂ packed needle trap for accurate and reliable sampling and analysis of the halogenated volatile organic compounds in air. *Int. J. Environ. Anal. Chem.* **101**, 263–280 (2021).
24. Firoozichahak, A. *et al.* Development of a needle trap device packed with titanium-based metal–organic framework sorbent for extraction of phenolic derivatives in air. *J. Sep. Sci.* **43**, 1011–1018 (2020).
25. Pirmohammadi, Z. *et al.* Determination of urinary methylhippuric acids using MIL-53-NH₂(Al) metal–organic framework in microextraction by packed sorbent followed by HPLC–UV analysis. *Biomed. Chromatogr.* **34**, e4725 (2020).
26. Saedi, N. *et al.* A needle trap device packed with MIL-100(Fe) metal organic frameworks for efficient headspace sampling and analysis of urinary BTEXs. *Biomed. Chromatogr.* **34**, e4800 (2020).
27. Langari, A. A. A., Firoozichahak, A., Alizadeh, S., Nematollahi, D. & Farhadian, M. Efficient extraction of aromatic amines in the air by the needle trap device packed with the zirconium based metal–organic framework sorbent. *RSC Adv.* **10**, 13562–13572 (2020).
28. Rahimpoor, R. *et al.* Bio-monitoring of non-metabolized BTEX compounds in urine by dynamic headspace-needle trap device packed with 3D Ni/Co-BTC bimetallic metal–organic framework as an efficient absorbent. *Microchem. J.* **166**, 106229 (2021).
29. Rahimpoor, R. *et al.* Determination of halogenated hydrocarbons in urine samples using a needle trap device packed with Ni/Zn-BTC bi-MMOF via the dynamic headspace method. *RSC Adv.* **11**, 21537–21547 (2021).
30. Al-Kutubi, H., Gascon, J., Sudhölter, E. J. & Rassaei, L. Electrosynthesis of metal–organic frameworks: challenges and opportunities. *ChemElectroChem* **2**, 462–474 (2015).
31. Ji, L., Wang, J., Wu, K. & Yang, N. Tunable electrochemistry of electrosynthesized copper metal–organic frameworks. *Adv. Funct. Mater.* **28**, 1706961 (2018).
32. Li, W. J., Tu, M., Cao, R. & Fischer, R. A. Metal–organic framework thin films: electrochemical fabrication techniques and corresponding applications & perspectives. *J. Mater. Chem. A* **4**, 12356–12369 (2016).
33. Alizadeh, S. & Nematollahi, D. Electrochemically assisted self-assembly technique for the fabrication of mesoporous metal–organic framework thin films: composition of 3D hexagonally packed crystals with 2D honeycomb-like mesopores. *J. Am. Chem. Soc.* **139**, 4753–4761 (2017).
34. Alizadeh, S. & Nematollahi, D. Convergent and divergent paired electrodeposition of metal–organic framework thin films. *Sci. Rep.* **9**, 1–13 (2019).
35. Martinez Joaristi, A., Juan-Alcañiz, J., Serra-Crespo, P., Kapteijn, F. & Gascon, J. Electrochemical synthesis of some archetypical Zn²⁺, Cu²⁺, and Al³⁺ metal organic frameworks. *Crystal Growth Des.* **12**, 3489–3498 (2012).
36. Cheng, X. *et al.* Erratum: Size- and morphology-controlled NH₂-MIL-53(Al) prepared in DMF water mixed solvents. *Dalton Trans.* **43**, 44944505 (2014).
37. Hod, I. *et al.* Directed growth of electroactive metal–organic framework thin films using electrophoretic deposition. *Adv. Mater.* **26**, 6295–6300 (2014).
38. Zhang, L. *et al.* NH₂-MIL-53 (Al) metal–organic framework as the smart platform for simultaneous high-performance detection and removal of Hg²⁺. *Inorg. Chem.* **58**, 12573–12581 (2019).
39. Bolinois, L. *et al.* Breathing-induced new phase transition in an MIL-53 (Al)-NH₂ metal–organic framework under high methane pressures. *Chem. Commun.* **53**, 8118–8121 (2017).
40. Emam, H. E., Ahmed, H. B., El-Deib, H. R., El-Dars, F. M. & Abdelhameed, R. M. Non-invasive route for desulfurization of fuel using infrared-assisted MIL-53(Al)-NH₂ containing fabric. *J. Colloid Interface Sci.* **556**, 193–205 (2019).
41. Guan, Y., Xia, M., Wang, X., Cao, W. & Marchetti, A. Water-based preparation of nano-sized NH₂-MIL-53(Al) frameworks for enhanced dye removal. *Inorg. Chim. Acta* **484**, 180–184 (2019).
42. Meng, T., Hao, Y.-N., Zheng, L. & Cao, M. Organophosphoric acid-derived CoP quantum dots@S, N-codoped graphite carbon as a trifunctional electrocatalyst for overall water splitting and Zn–air batteries. *Nanoscale* **10**, 14613–14626 (2018).
43. Wang, Y., Liu, B. Y., Yang, G. & Chai, Z. Synthesis of 2-aminophosphates via S_N²-type ring openings of aziridines with organophosphoric acids. *Org. Lett.* **21**, 4475–4479 (2019).
44. Lopes, T. R. *et al.* Multinuclear magnetic resonance study on the occurrence of phosphorus in activated carbons prepared by chemical activation of lignocellulosic residues from the babassu production. *J. Environ. Chem. Eng.* **5**, 6016–6029 (2017).
45. Das, S. *et al.* Extraction of scandium (III) from acidic solutions using organo-phosphoric acid reagents: A comparative study. *Sep. Purif. Technol.* **202**, 248–258 (2018).
46. Sato, T. *et al.* Investigation of the hemolytic effects of various organophosphoric acid triesters (OPEs) and their structure-activity relationship. *Toxicol. Environ. Chem.* **59**, 305–313 (1997).
47. Sepehrmansouri, H. *et al.* Multilinker phosphorous acid anchored En/MIL-100(Cr) as a novel nanoporous catalyst for the synthesis of new N-heterocyclic pyrimido [4, 5-*b*] quinolines. *Mol. Catal.* **481**, 110303 (2020).
48. Babaei, S., Zarei, M., Sepehrmansourie, H., Zolfigol, M. A. & Rostamnia, S. Synthesis of metal–organic frameworks MIL-101(Cr)-NH₂ containing phosphorous acid functional groups: Application for the synthesis of N-Amino-2-pyridone and pyrano [2, 3-*c*] pyrazole derivatives via a cooperative vinylogous anomeric-based oxidation. *ACS Omega* **5**, 6240–6249 (2020).
49. Moradi, S., Zolfigol, M. A., Zarei, M., Alonso, D. A. & Khoshnood, A. Synthesis of a biological-based glycoluril with phosphorous acid tags as a new nanostructured catalyst: Application for the synthesis of novel natural henna-based compounds. *ChemistrySelect* **3**, 3042–3047 (2018).
50. Afsar, J. *et al.* Synthesis and application of melamine-based nano catalyst with phosphonic acid tags in the synthesis of (3'-indolyl) pyrazolo [3, 4-*b*] pyridines via vinylogous anomeric based oxidation. *Mol. Catal.* **482**, 110666 (2020).
51. Jalili, F., Zarei, M., Zolfigol, M. A., Rostamnia, S. & Moosavi-Zare, A. R. SBA-15/PrN (CH₂PO₃H₂)₂ as a novel and efficient mesoporous solid acid catalyst with phosphorous acid tags and its application on the synthesis of new pyrimido [4,5-*b*] quinolones and pyrido [2,3-*d*] pyrimidines via anomeric based oxidation. *Microporous Mesoporous Mater.* **294**, 109865 (2020).
52. Hargrove, T. Y. *et al.* Complexes of *Trypanosoma cruzi* sterol 14 α -demethylase (CYP51) with two pyridine-based drug candidates for Chagas disease: structural basis for pathogen selectivity. *J. Biol. Chem.* **288**, 31602–31615 (2013).
53. Chaban, T., Matiychuk, V., Ogurtsov, V., Chaban, I. & Nektgayev, I. Development of effective anti-inflammatory drug candidates among novel thiazolopyridines. *Ukrain. Biochem. J.* **92**, 132–139 (2020).
54. Adibian, F., Pourali, A. R., Maleki, B., Baghayeri, M. & Amiri, A. One-pot synthesis of dihydro-1H-indeno [1,2-*b*] pyridines and tetrahydrobenzo [b] pyran derivatives using a new and efficient nanocomposite catalyst based on N-butylsulfonate-functionalized MMWCNTs-D-NH₂. *Polyhedron* **175**, 114179 (2020).
55. Grivsky, E. M., Lee, S., Sigel, C. W., Duch, D. S. & Nichol, C. A. Synthesis and antitumor activity of 2,4-diamino-6-(2,5-dimethoxybenzyl)-5-methylpyrido [2,3-*d*] pyrimidine. *J. Med. Chem.* **23**, 327–329 (1980).
56. Deb, M. L. & Bhuyan, P. J. Synthesis of novel classes of pyrido [2,3-*d*] pyrimidines, Pyrano [2,3-*d*] pyrimidines, and pteridines. *Synth. Commun.* **36**, 3085–3090 (2006).

57. Devi, I., Borah, H. N. & Bhuyan, P. J. Studies on uracils: a facile one-pot synthesis of oxazino [4,5-*d*]-, pyrano [2,3-*d*]-, pyrido [2,3-*d*]-and pyrimido [4,5-*d*] pyrimidines using microwave irradiation in the solid state. *Tetrahedron Lett.* **45**, 2405–2408 (2004).
58. Ibrahim, B. A. & Mohareb, R. M. Uses of ethyl benzoyl acetate for the synthesis of thiophene, pyran, and pyridine derivatives with antitumor activities. *J. Heterocycl. Chem.* **57**, 4023–4035 (2020).
59. Mohareb, R. M. & Mikhail, I. R. Synthesis of Thiazole, Thiophene, pyran and pyridine derivatives derived from 3-phenyl-1*H*-pyrazol-5(4*H*)-one with anti-proliferative, tyrosine kinase and PIM-1 kinase inhibitions. *Lett. Drug Des. Discov.* **17**, 485–501 (2020).
60. Allais, C., Grassot, J. M., Rodriguez, J. & Constantieux, T. Metal-free multicomponent syntheses of pyridines. *Chem. Rev.* **114**, 10829–10868 (2014).
61. Alabugin, I. V. *Stereoelectronic Effects: A Bridge Between Structure and Reactivity* (Wiley, 2016).
62. Yarie, M. Catalytic anomeric based oxidation. *Iranian Journal of Catalysis* **7**, 85–88 (2017).
63. Yarie, M. Spotlight: Catalytic vinylogous anomeric based oxidation (Part I). *Iran. J. Catal.* **10**, 79–83 (2020).
64. Bai, C. B., Wang, N. X., Xing, Y. & Lan, X.-W. Progress on chiral NAD(P)H model compounds. *Synlett* **13**, 402–414 (2017).
65. He, T. *et al.* Base-promoted cascade approach for the preparation of reduced Knoevenagel adducts using hantzsch esters as reducing agent in water. *Synlett* **27**, 1864–1869 (2016).
66. Hamasaka, G., Tsuji, H. & Uozumi, Y. Organoborane-catalyzed hydrogenation of unactivated aldehydes with a Hantzsch ester as a synthetic NAD(P)H analogue. *Synlett* **26**, 2037–2041 (2015).
67. Bodaghifard, M. A. & Shafi, S. Ionic liquid-immobilized hybrid nanomaterial: An efficient catalyst in the synthesis of benzimidazoles and benzothiazoles via anomeric-based oxidation. *J. Iran. Chem. Soc.* **18**, 677–687 (2021).
68. Bagheri, S., Zolfigol, M. A. & Maleki, F. [TEATNM] and [TEATCM] as novel catalysts for the synthesis of pyridine-3, 5-dicarbonylnitriles via anomeric-based oxidation. *New J. Chem.* **41**, 9276–9290 (2017).
69. Shiri, M. Indoles in multicomponent processes (MCPs). *Chem. Rev.* **112**, 3508–3549 (2012).
70. Shiri, M., Zolfigol, M. A., Kruger, H. G. & Tanbakouchian, Z. Bis- and trisindolylmethanes (BIMs and TIMs). *Chem. Rev.* **110**, 2250–2293 (2010).
71. Al-Matar, H. M., Adam, A. Y., Khalil, K. D. & Elnagdi, M. H. Studies with 3-oxoalkanenitriles: Novel rearrangements observed while exploring the utility of 2-cyanoacetyl-1-methylpyrrole as a precursor to pyrrole substituted heterocyclic compounds. *ARKIVOC* **6**, 1–15 (2012).
72. Zhang, S., Zhou, L. & Chen, M. Amine-functionalized MIL-53(Al) with embedded ruthenium nanoparticles as a highly efficient catalyst for the hydrolytic dehydrogenation of ammonia borane. *RSC Adv.* **8**, 12282–12291 (2018).
73. Chen, J., Xu, Y., Li, S., Xu, F. & Zhang, Q. Ratio fluorescence detection of tetracycline by a Eu³⁺/NH₂-MIL-53(Al) composite. *RSC Adv.* **11**, 2397–2404 (2021).
74. Xu, S. & Ni, Y. NH₂-MIL-53(Al) nanocrystals: A fluorescent probe for the fast detection of aromatic nitro-compounds and ions in aqueous systems. *Analyst* **144**, 1687–1695 (2019).
75. Li, C., Xiong, Z., Zhang, J. & Wu, C. The strengthening role of the amino group in metal-organic framework MIL-53(Al) for methylene blue and malachite green dye adsorption. *J. Chem. Eng. Data* **60**, 3414–3422 (2015).
76. Seoane, B., Téllez, C., Coronas, J. & Staudt, C. NH₂-MIL-53(Al) and NH₂-MIL-101(Al) in sulfur-containing copolyimide mixed matrix membranes for gas separation. *Sep. Purif. Technol.* **111**, 72–81 (2013).
77. Serra-Crespo, P. *et al.* NH₂-MIL-53(Al): A high-contrast reversible solid-state nonlinear optical switch. *J. Am. Chem. Soc.* **134**, 8314–8317 (2012).
78. Stavitski, E. *et al.* Complexity behind CO₂ capture on NH₂-MIL-53(Al). *Langmuir* **27**, 3970–3976 (2011).
79. Babae, S., Zolfigol, M. A., Zarei, M. & Zamanian, J. 1,10-Phenanthroline-based molten salt as a bifunctional sulfonic acid catalyst: Application to the synthesis of N-heterocycle compounds via anomeric based oxidation. *ChemistrySelect* **3**, 8947–8954 (2018).
80. Alabugin, I. V. *et al.* Stereoelectronic power of oxygen in control of chemical reactivity: the anomeric effect is not alone. *Chem. Soc. Rev.* <https://doi.org/10.1039/D1CS00386K> (2021).
81. Sepehrmansourie, H., Zarei, M., Zolfigol, M. A., Babae, S. & Rostamnia, S. Application of novel nanomagnetic metal-organic frameworks as a catalyst for the synthesis of new pyridines and 1,4-dihydropyridines via a cooperative vinylogous anomeric based oxidation. *Sci. Rep.* **11**, 1–15 (2021).
82. Zolfigol, M. A. Silica sulfuric acid/NaNO₂ as a novel heterogeneous system for production of thionitriles and disulfides under mild conditions. *Tetrahedron* **57**, 9509–9511 (2001).
83. Rajabi-Salek, M., Zolfigol, M. A. & Zarei, M. Synthesis of a novel DABCO-based nanomagnetic catalyst with sulfonic acid tags: Application to the synthesis of diverse spiropyrans. *Res. Chem. Intermed.* **44**, 5255–5269 (2018).
84. Zarei, M., Zolfigol, M. A., Moosavi-Zare, A. R. & Noroozizadeh, E. Trityl bromide versus nano-magnetic catalyst in the synthesis of henna-based xanthenes and bis-coumarins. *J. Iran. Chem. Soc.* **14**, 2187–2198 (2017).
85. Zarei, M., Sepehrmansourie, H., Zolfigol, M. A., Karamian, R. & Farida, S. H. M. Novel nano-size and crab-like biological-based glycoluril with sulfonic acid tags as a reusable catalyst: Its application to the synthesis of new mono- and bis-spiropyrans and their in vitro biological studies. *New J. Chem.* **42**, 14308–14317 (2018).
86. Moosavi-Zare, A. R. *et al.* Design, characterization and application of new ionic liquid 1-sulfolpyridinium chloride as an efficient catalyst for tandem Knoevenagel-Michael reaction of 3-methyl-1-phenyl-1*H*-pyrazol-5(4*H*)-one with aldehydes. *Appl. Catal. A* **467**, 61–68 (2013).
87. Noroozizadeh, E. *et al.* Synthesis of bis-coumarins over acetic acid functionalized poly(4-vinylpyridinium) bromide (APVPB) as a green and efficient catalyst under solvent-free conditions and their biological activity. *J. Iran. Chem. Soc.* **15**, 471–481 (2018).

Acknowledgements

We thank the Bu-Ali Sina University and Iran National Science Foundation (INSF) (Grant Number: 98001912) for financial support.

Author contributions

S.K., H.S. S.A and M.Z.; methodology, validation, investigation, writing the original draft. M.A.Z.; supervision, resources, project administration, funding acquisition, conceptualization, writing-review. D.N., H.S and J.A. supervision, conceptualization of electrosynthesis parts and writing-review and editing.

Competing interests

The authors declare no competing interests.

Additional information

Supplementary Information The online version contains supplementary material available at <https://doi.org/10.1038/s41598-021-97801-7>.

Correspondence and requests for materials should be addressed to M.Z., M.A.Z., D.N., S.A. or H.S.

Reprints and permissions information is available at www.nature.com/reprints.

Publisher's note Springer Nature remains neutral with regard to jurisdictional claims in published maps and institutional affiliations.



Open Access This article is licensed under a Creative Commons Attribution 4.0 International License, which permits use, sharing, adaptation, distribution and reproduction in any medium or format, as long as you give appropriate credit to the original author(s) and the source, provide a link to the Creative Commons licence, and indicate if changes were made. The images or other third party material in this article are included in the article's Creative Commons licence, unless indicated otherwise in a credit line to the material. If material is not included in the article's Creative Commons licence and your intended use is not permitted by statutory regulation or exceeds the permitted use, you will need to obtain permission directly from the copyright holder. To view a copy of this licence, visit <http://creativecommons.org/licenses/by/4.0/>.

© The Author(s) 2021